Realia et naturalia

DISSERTATIONES
PHYSICAE
UNIVERSITATIS
TARTUENSIS
94

MIHKEL PAJUSALU

Localized Photosynthetic Excitons

DISSERTATIONES PHYSICAE UNIVERSITATIS TARTUENSIS
94

DISSERTATIONES PHYSICAE UNIVERSITATIS TARTUENSIS
94

MIHKEL PAJUSALU

Localized Photosynthetic Excitons

UNIVERSITY OF TARTU
PRESS
1632

This study was carried out at the University of Tartu, Institute of Physics.

The Dissertation was admitted on August 26, 2014, in partial fulfillment of the requirements for the degree of Doctor of Philosophy in physics, and allowed for defense by the Council of the Institute of Physics, University of Tartu.

Supervisors: DSc Arvi Freiberg, University of Tartu, Estonia
PhD Margus Rätsep, University of Tartu, Estonia

Opponents: Habil. Dr. Leonas Valkunas, Vilnius University and Center for Physical Sciences and Technology, Lithuania
DSc Georg Liidja, National Institute of Chemical Physics and Biophysics, Estonia

Defense: 31. October 2014

This work has been partially supported by graduate school "Functional materials and technologies", receiving funding from the European Social Fund under project 1.2.0401.09-0079 in Estonia.

ISSN 1406-0647
ISBN 978-9949-32-667-9 (print)
ISBN 978-9949-32-668-6 (pdf)

University of Tartu Press
www.tyk.ee

CONTENTS

LIST OF ORIGINAL PUBLICATIONS

This thesis is based on the following publications (full texts included at the end of the thesis), which are referred to in the text by their Roman numerals.

I M. Rätsep, M. Pajusalu and A. Freiberg. "Wavelength-dependent electron–phonon coupling in impurity glasses," *Chemical Physics Letters*, vol. 479, no. 1, pp. 140–143, 2009.

II M. Pajusalu, M. Rätsep, G. Trinkunas and A. Freiberg. "Davydov splitting of excitons in cyclic bacteriochlorophyll a nanoaggregates of bacterial light-harvesting complexes between 4.5 and 263 K," *ChemPhysChem*, vol. 12, no. 3, pp. 634–644, 2011.

III A. Freiberg, M. Pajusalu, M. Rätsep. "Excitons in intact cells of photosynthetic bacteria," *Journal of Physical Chemistry B*, vol. 117, no. 38, pp. 11007–11014, 2013.

IV M. Pajusalu, M. Rätsep, A. Freiberg. "Temperature dependent electron–phonon coupling in chlorin-doped impurity glass and in photosynthetic FMO protein containing bacteriochlorophyll a," *Journal of Luminescence*, vol. 152, pp. 79–83, 2014.

V M. Rätsep, M. Pajusalu, J. M. Linnanto, A. Freiberg. "Subtle spectral effects accompanying the assembly of bacteriochlorophylls into cyclic light harvesting complexes revealed by high-resolution fluorescence spectroscopy", submitted to *The Journal of Chemical Physics*), 13. May 2014, currently in second review (second review version is included in the print version).

VI M. Pajusalu, R. Kunz, M. Rätsep, K. Timpmann, J. Köhler, A. Freiberg, "Unified analysis of ensemble and single-complex spectral data on light harvesting 2 chromoproteins to gain deeper insight into bacterial photosynthesis", to be submitted to *The New Journal of Physics.*

AUTHOR'S CONTRIBUTION

I Performing a part of the spectral hole-burning and difference fluorescence line-narrowing experiments (on chlorin samples), partial fitting of the experimental data.

II Assembling the theoretical model, improving the experimental apparatus, conducting most of the experiments, analyzing the experimental data using the model, writing a draft of the article.

III Performing the measurements, analyzing the data, writing a large part of the article.

IV Developing the model for fitting the experimental spectra, fitting the spectra, analyzing the results and writing parts of the article.

V Some calculations (fitting) and contributions to the text.

VI Developing the theoretical model, analyzing the data according to the model, writing a draft of the article.

ABBREVIATIONS AND SYMBOLS

BChl a	bacteriochlorophyll a
ΔFLN	difference fluorescence line-narrowing
DOS	density of states
FFT	fast Fourier transform
FLN	fluorescence line-narrowing
FMO	Fenna-Matthews-Olson complex
FWHM	full width at half-maximum
IDF	inhomogeneous distribution function
LH	light-harvesting
LH1	light-harvesting complex 1
LH2	light-harvesting complex 2
PSB	phonon sideband
RC	reaction center
SDF	spectral density function
SSH	Su-Schrieffer-Heeger
ZPL	zero-phonon line
a.u.	arbitrary unit

1 INTRODUCTION

1.1 Aspects of quantum mechanics in living nature

It would be expected that on the most basic level of life – on the scale of the proteins and protein complexes that perform all processes needed for sustaining living organisms – the rules of classical physics would start to lose their applicability and quantum mechanical effects would emerge. At nanoscopic scales, wave-matter duality, quantization of energy, quantum statistics and other effects would need to be taken into account. However, the constituents of living cells are in perpetual motion and constantly changing, disturbing the order needed for more interesting quantum mechanical effects to appear. Therefore, there were objections to the use of quantum mechanics to explain biology [1]. Still, several non-trivial effects involving living nature or its constituents have been found since [2,3], such as photon antibunching [4], matter-wave nature of biomolecules [5], quantum algorithms running on biomolecules [6], and quantum tunnelling in enzymatic reactions [7,8]. However, these processes were generally studied at very low temperatures and in artificial conditions, raising questions about the significance of quantum mechanics on the level of living cells. In this work we study the quantum mechanics in bacterial photosynthesis and, among other things, prove that excitons [9] are relevant for living organisms.

Photosynthesis, the main theme of this research, is one of the most important processes in the biosphere, supplying almost all of the life on the Earth with energy by converting the flux of photons coming from the Sun into chemical energy. Still, photosynthesis is not fully understood, partly since its origins lie deep within quantum mechanics [9–12]. One of the quantum mechanical processes useful for understanding photosynthesis, especially in purple bacteria, is the formation of excitons [9]. Excitons are collective excitations of several molecules simultaneously, allowing transfer of energy without transfer of charges. The excitonic model was developed by Frenkel over eighty years ago in regular crystals [13], but later the same effects have been found in low-temperature samples extracted from biological organisms [9,14–16], and their synthetic analogues [17]. Recently, there has even been evidence of coherent energy transfer in subparts of photosynthetic units at physiological temperatures [18–20], but these artificial environments could lead to artefacts and therefore do not prove the presence of excitons in living organisms conclusively.

The main counterpoint against the presence of excitons, as in general with more complex quantum-mechanical effects in living organisms, is that the insides of living cells are very dynamic and chaotic and this would lead to the destruction of the intricate phase relationships that are required for these effects to survive [9,21–24]. One of such problems is the energy of thermal fluctuations that increases with the increase of temperatures. Very generally, the energy of thermal fluctuations can be approximated with $k_{\mathrm{B}}T$, the product of the

Boltzmann constant and the absolute temperature. At low temperatures, this is negligible, being about 3 cm^{-1} at 4.2 K, the boiling point of helium at the atmospheric pressure, but increases to 200 cm^{-1} at room temperature.

In this work we study excitons in bacterial photosynthesis and investigate their behaviour in increasingly complex biological structures and at temperatures ranging from near absolute zero to physiological temperatures. We employ experimental methods (optical spectroscopy) and explain the results using theoretical modelling. This should show how resilient the excitons are to disturbances and therefore how applicable they are for studying the operating principles of life.

1.2 Light-harvesting apparatus of purple bacteria

Bacteria are very efficient at photosynthesis, but the exact processes behind this are not yet completely known. In purple bacteria the prevalent theory is that the energy is primarily absorbed in the light-harvesting antenna complexes (LH complexes, see Fig. 1.1) [14,30], where it is captured as excitons [9]. The excitons transfer towards energetically lower complexes until they reach the reaction centre (RC), where the energy is used to perform a chemical reaction. This, however, is based on extrapolation of low-temperature studies.

In this work we study the operation of light-harvesting complexes from two species of purple bacteria: *Rhodopseudomonas acidophila* and *Rhodobacter sphaeroides*. These bacterial species contain symmetrical antenna complexes, which capture the photons in the form of excitons [9,14]. The main types of such complexes are the LH1 and LH2 complexes that contain highly regular arrays of bacteriochlorophyll a (BChl a) molecules, which seem ideal for facilitating collective excitations [30].

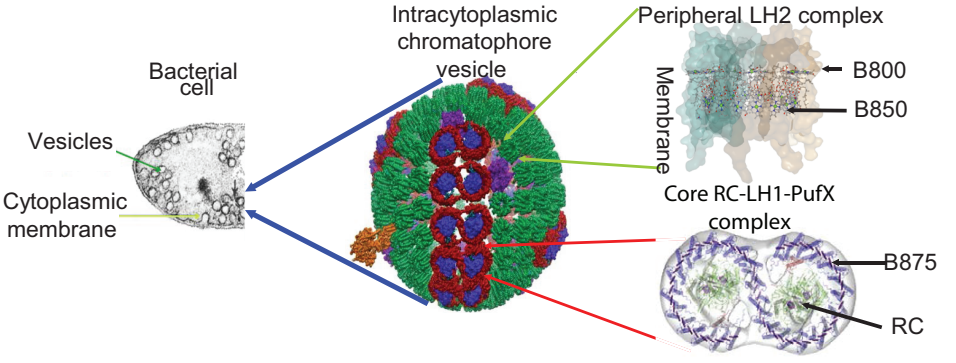

Figure 1.1. LH complexes in bacterial cells [25]. The complexes are situated mostly on the surface of intracytoplasmic chromatophore vesicles [26]. Different important parts of RC-LH1-PufX [27] and LH2 [28,29] complexes (B800, B850 and B875 rings alongside with reaction centres RC) have been brought out [25].

The LH1 complexes are naturally found in a dimeric RC-LH1-PufX configuration, containing two semi-circular arrays of BChl a molecules that have been joined into an S-shaped B875 antenna around two RC units [27,31,32] (see Fig. 1.1). The LH2 complexes contain two circular arrays of BChl a molecules: the B800 ring close to the cytoplasmic side of the complex with 9 pigment molecules, and the B850 circle containing 18 pigment molecules in 9 dimeric subunits [33]. The energy absorbed in the complexes is funnelled into the RC, where it facilitates electron transfer processes [34,35]. The photosynthetic membranes, on which the complexes reside, self-assemble into photosynthetic membrane vesicles [26].

In this work, we study both the LH1 and LH2 complexes in different configurations and environments [25], but concentrate on the B850 circle of *Rps. acidophila* in theoretical analysis, since its structure is well known [28,36,37] and therefore it has been the object of many studies [14,38–41].

Excitons have been studied in these complexes for a long time [9,14–16] and it has been proposed that the electron-phonon coupling present in the complexes leads to the self-trapping of excitons [42–47].

1.3 Overview of LH2 and its spectroscopic properties

The LH2 complexes of *Rps. acidophila* consist of 9 dimeric subunits (labelled as α and β, see Fig. 1.2), each dimer containing three BChl a molecules [14]. The X-ray diffraction crystal structure of this complex has been determined to 2.0 Å resolution and the initial model has also been computationally optimized [28,36,37]. The structure of the LH2 complexes of *Rb. sphaeroides* is expected to be similar, although its crystal structure has never been published (nor measured to our knowledge); this is also a reason why we concentrated on the *Rps. acidophila* LH2 in theoretical analysis.

The BChl a molecules within the complex have four major transition dipoles: B_y and B_x in the ultraviolet spectral region (forming the Soret band), Q_x in the visible wavelength range, and Q_y in the near-infrared [14]. In this work, we concentrate only on the Q_y transition dipole moments of the BChl a molecules. We also do not consider the carotenoids within the LH2.

The 27 BChl a molecules within the LH2 complex can be assigned into two sub-assemblies, the B800 and the B850 rings, based on the respective peak positions of their ensemble absorption spectra in near-infrared (about 800 and 850 nm, respectively, see Fig. 1.3). The B800 sub-assembly contains 9 BChl a molecules and the B850 18 BChl a molecules. The assemblies have also very different spectroscopic properties.

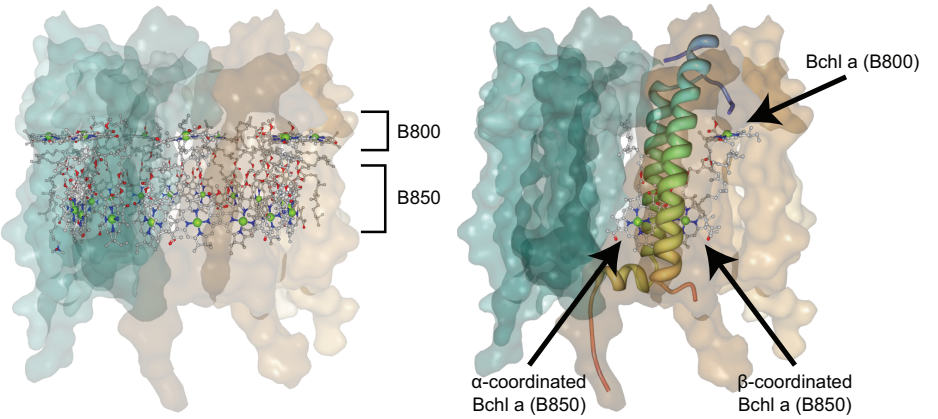

Figure 1.2. A complete LH2 complex, showing the B800 and B850 BChl a assemblies (left) and a single dimeric subunit within the complex (right) [28,29,48]. On the right, the locations of α- and β-coordinated B850 BChl a molecules are shown alongside with a single B800 BChl a. The helix on the front belongs to the α and the helix on the back to the β chain.

The transition dipoles of the pigments in the B800 ring are weakly coupled, producing a single absorption peak (in ensemble spectra) at around 800 nm. The B850 complex, on the other hand, features very strong excitonic interaction between the Q_y transitions [9,15] (based on low-temperature studies). This is due to the close arrangement of the pigments (about 0.9 nm between the pigments within a single dimer and 1 nm between the pigments of adjacent dimers [36,37,49–51]); the coupling strengths between the Q_y dipoles within the α-β dimer have been estimated to be between 200 and 550 cm^{-1} [16,49,51–54]. As a result, 18 excitonic energy levels are formed in each B850 ring, producing two peaks in the absorption spectrum, one is the B850 band and the other, much weaker, overlaps with the B800 band (can only be detected using very specific techniques, such as femtosecond pump-probe transient analysis [55] or fluorescence excitation anisotropy, see description and references below). This splitting phenomenon is also called Davydov splitting [22] (as we reference in the title of Paper II).

In this work, especially in the theoretical analysis, we concentrate on the B850 rings and consider them separately from the B800 rings, since the excitations within the B800 ring are transmitted to the B850 ring within 1 ps [56]. Due to this, the absorption spectra generated by us never contain the B800 peak.

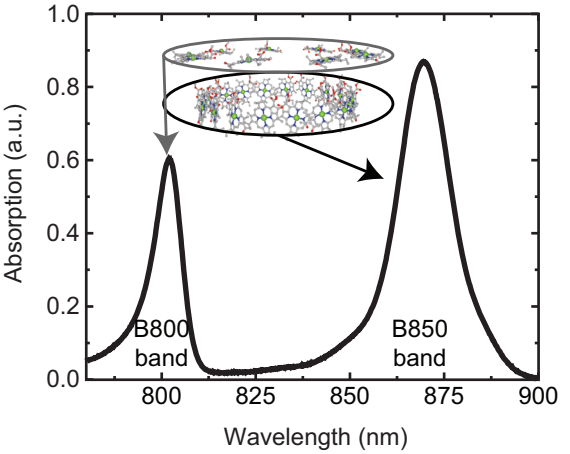

Figure 1.3. B800 and B850 bands in the absorption spectrum of *Rps. acidophila* [16] alongside with a representation of the BChl a cores [28,48]. We only concentrate on the Q_y transitions of BChl a in the near-infrared.

In the B850 rings, it is also important to note that the α- and β-coordinated BChl a molecules are both in different microenvironments, causing α-coordinated molecules to have higher site excitation energies and affecting resulting spectra [57]. When we consider a single α-β dimer in a perfectly ordered average LH2 structure, it is convenient to distinguish between the average of and the difference between the excitation energies of the α- and β-coordinated pigments. The average excitation energies of the BChl a sites have been estimated to range from 12160 to 12810 cm^{-1} and the energetic differences between them from 0 to 532 cm^{-1} [16,52,54,58,59]. In our works we found the energy splitting to be around 100 cm^{-1} (Papers VI), in Paper II we proposed around 300 cm^{-1}, but this earlier result seems unrealistic when the single-complex data are taken into account. Also, the orientations of the transition dipoles of the pigments differ between the sites. However, it has been proven that in reality the complexes are spatially distorted and the symmetry is broken, leading to hypotheses about elliptical deformations [60–63] (symmetry is achieved in the crystal structure due to averaging over a large number of complexes), but still the perfectly ordered structure can be used as the basis to which different disorder models are added.

The 18 excitonic states formed in the B850 ring can be indexed either from $k = 0$, $k = \pm 1$ to $k = \pm 8$, $k = 9$ [9] (see Fig. 1.4 (a)) or from $k = 0$ to 17. The ± indexing is justified in a perfect complex with no disorder (± states are energetically degenerate, only the dipole moment directions differ). When disorder is added, each state (numbered according to energy) will have its own distribution of energetic states, leading to 18 continuous distributions of states in an ensemble of pigments, see Fig. 1.4 (b).

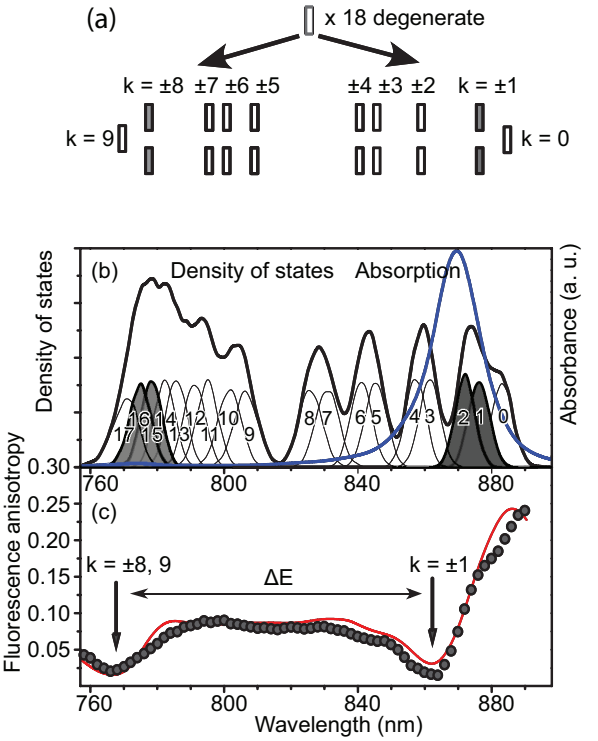

Figure 1.4. Part (a) shows the splitting of the 18 degenerate excitation energies of the BChl a molecules in B850 ring into 18 excitonic states, due to excitonic interaction. By adding disorder, we can produce a density of states distribution for each excitonic level. In part (b), we show the density of states individually (black narrow lines, numbered to show the $k = 0$–17 convention) and summed (black thick line). Absorption is shown as the blue line. The lines corresponding to the $k = 1$, 2, 15 and 16 states have been filled with gray to signify the main states contributing to absorption. The energetic positions of the lowest and highest exciton states, along with their energetic difference, can be estimated from fluorescence excitation anisotropy (panel (c), scatter plot is experimental 4.5 K anisotropy, red line is the modelled anisotropy) [64].

Of the 18 states, the primary absorbing states are the $k = 1$ and $k = 2$, which give rise to most of the B850 band absorption, although other states also contribute. In Paper VI, we show that even the $k = 0$ can give a significant contribution to absorption in case of strongly self-trapped states. On the shorter wavelength side, the primary absorbers are the $k = 15$ and $k = 16$ states that form a faint absorbance band beneath the B800 band, which is not distinguishable in absorption spectra. The emission appears from the energetically lowest states within the state manifold, being almost exclusively from $k = 0$ at low temperatures.

The excitonic properties can experimentally studied by polarization-dependent studies [9], such as fluorescence excitation anisotropy [65,66], linear

dichroism, and circular dichroism [58,67]. Both of the edges of the exciton manifold are still clearly distinguishable in fluorescence excitation anisotropy (see Fig. 1.4 (c)) [65,66]. The results of this analysis have been also confirmed by femtosecond pump-probe transient spectra that appear to show the higher-energy excitonic absorption band [55].

Another broad area of LH complex research concerns their excited state lifetimes, energy transfer, and temporal dynamics. This has been both studied experimentally and theoretically very widely [38,53,56,66,68–79], but we do not focus on these aspects in this work.

The most precise methods for estimating the excitonic structure within the complex come from quantum chemistry [43,53,80–82]. These have been used widely, but they are generally too computationally intensive to be used for large-scale Monte Carlo spectral simulations that take into account a large number of disorder configurations. Therefore, it is needed to resort to simpler methods, such as dipole-dipole approximation, for larger-scale simulations [16,38,62,83,84]. We will elaborate on this in the theoretical model section, as the dipole-dipole approximation of coupling energies was the main theoretical tool in our calculations.

Historically, the LH complexes have been mostly studied in large ensembles, but now also experimental results on single separated complexes are available [61,62,85–98] (see Fig. 1.5). When each single complex is studied individually, more interesting effects appear, such as the splitting of the B850 and B800 absorption bands into sub-bands [60,61,88–90,99]. Single-molecule data will be studied in more detail in the part discussing Paper VI.

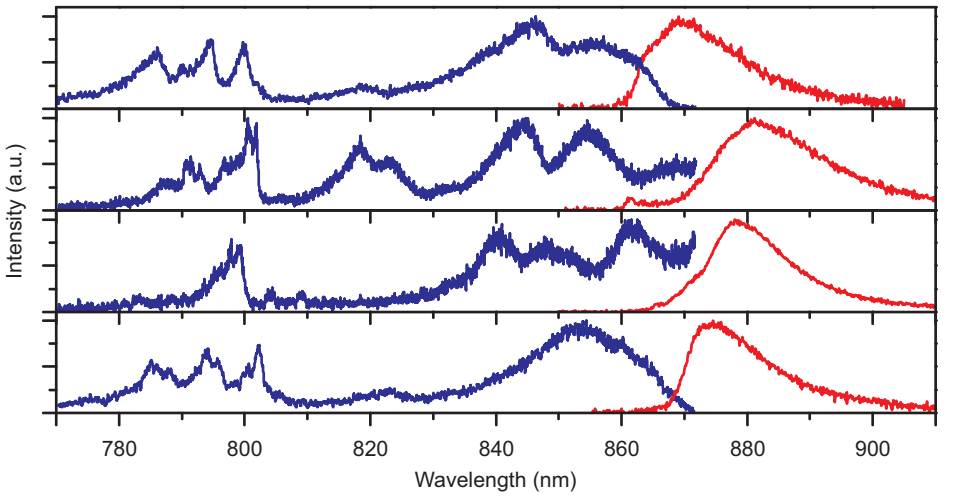

Figure 1.5. Example spectra of single LH2 complexes of *Rps. acidophila*, integrated over time (see Paper VI). Excitation spectra are shown as blue lines (directly comparable to absorption spectra due to low optical density). Fluorescence spectra are shown in red. The level of detail seen is far greater than in the ensemble measurements.

1.4 Spectroscopic methods and setups used in this work

1.4.1 Absorption and fluorescence spectroscopy

Some form of absorption or fluorescence spectroscopy was used for either general characterization of the samples or for getting reference for modelling (especially in the case temperature dependencies in Paper II) in all papers.

For absorption measurements, we used a high-stability tungsten light source BPS100 (BWTek, USA) with filters for shaping its spectrum.

For non-selective fluorescence measurements we used a 450 nm light-emitting diode or a 405 nm diode laser. Sample fluorescence was collected at a 90° angle in respect to excitation.

All the measurements were performed using Shamrock SR-303i 0.3 m spectrograph (Andor Technology, UK), which was equipped with an electrically cooled CCD camera (DV420A-OE, Andor Technology, UK).

1.4.2 Difference fluorescence line narrowing spectroscopy

One of the most precise ways of studying phonon sidebands and vibrational satellites is difference fluorescence line-narrowing (ΔFLN) spectroscopy [100–102], which combines together both the fluorescence line narrowing and spectral hole-burning methods. This technique relies on taking two fluorescence measurement at the same exciting wavelength with a spectrally narrow laser, separated by a period of hole-burning (at the same exciting frequency), and finding their difference. For these measurements, we used either a dye laser (Spectra Physics 375) or a Ti-sapphire laser (Spectra Physics 3900S). These measurements yield results only if a considerable portion of the pigments is bleached out during the hole-burning step and the emission is weakened due to this (this means also that the role of the bleached-out pigments must not be replaced by other pigments due to spectral diffusion).

As a complementary technique, we used spectral hole-burning. For this method, absorption spectra of the sample are measured both before and after bleaching with a spectrally narrow laser (the spectral linewidth of the lasers we used was <0.5 cm^{-1}). The difference between these two absorption spectra reveals the population of pigments bleached out during the process. From the spectral hole-burning, we primarily determined the location and width of the inhomogeneous distribution function (IDF) by bleaching a series of holes into the absorption spectrum (see the inset in Fig. 1.6).

The fluorescence line-narrowed spectra were used to determine characteristics of the exciton-phonon coupling through fitting of the spectra, according to equation (4.12) or by directly calculating the Huang-Rhys factors [103] using equation (3.19).

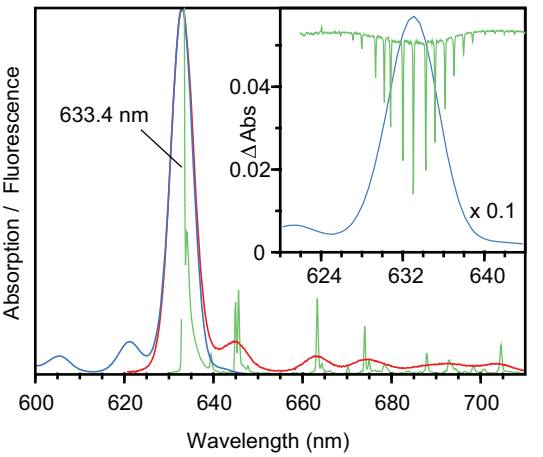

Figure 1.6. Spectral hole-burning and difference line-narrowing of chlorin-doped propanol-1 glass from Paper I [104]. The inset shows the depth of spectral holes in the absorption spectrum, giving direct evidence of the position and width of the IDF. The main figure shows the absorption (blue) and fluorescence (red) alongside with a ΔFLN spectrum (green). Note the fine structure revealed.

In Paper I [104], we studied the phonon sidebands in impurity glasses, such as chlorin (7,8-dihydroporphin) and chlorophyll a in 1-propanol at low temperatures. In Paper IV we studied the temperature dependency of chlorin and FMO complexes and in Paper V precise details about the behaviour of Huang-Rhys factors when the chlorophyll molecules are inserted into the protein matrix of an LH complex.

1.4.3 Fluorescence excitation anisotropy

A good technique for studying the excitonic structure of LH complexes is fluorescence excitation anisotropy [9,65,105]. In this method, a sample is excited with a linearly polarized light source and the fluorescence signal is collected through two polarizers, one polarized in parallel to the excitation and another in perpendicular. Then, the fluorescence excitation anisotropy value for each wavelength λ can be calculated as:

$$r(\lambda) = \frac{IF_{vv}(\lambda) - IF_{vh}(\lambda)}{IF_{vv}(\lambda) + 2IF_{vh}(\lambda)}. \tag{1.1}$$

In the equation 1.1, $IF_{vv}(\lambda)$ and $IF_{vh}(\lambda)$ are integrated fluorescence signals detected through a polarizer polarized in parallel or perpendicularly, respectively, to the polarization of the exciting laser. The theory can be read in more detail in the spectral simulations section. The spectral integration window can be chosen to select specific constituents within the sample, see Paper III for an analysis.

For our work, we developed a system for measuring such spectra automatically (see Fig. 1.7). The system consists of a motorized Ti-sapphire laser, which is tuned and controlled automatically by using a wavemeter for feedback.

The laser passes through a computer-controlled shutter and a passive iris, after which it is split between a beam that goes to a powermeter and a beam that excites the sample. Emission from the sample is collected through motorized polarizers. During the experiment the laser automatically scans the required wavelength range in steps. In each step the emission from the sample is collected through a polarizer that is polarized perpendicularly compared to the exciting laser and through a polarizer that is polarized in parallel to the excitation. The emission spectra are then integrated and the anisotropy is calculated according to the equation (1.1). All in all, this allows collecting anisotropy spectra with minimal human interaction.

The 90° geometry between the exciting laser and collection of emission allows eliminating most of the exciting laser from the measured spectrum and thus lowpass filters for blocking out the exciting laser before the monochromator are not needed.

The system can also be customized to measure in 0° and 180° geometries between the exciting laser and detection of fluorescence by using different mirror set-ups near the cryostat. This, for example, permits to measure fluorescence excitation anisotropy in high-pressure cells, not described in the present work.

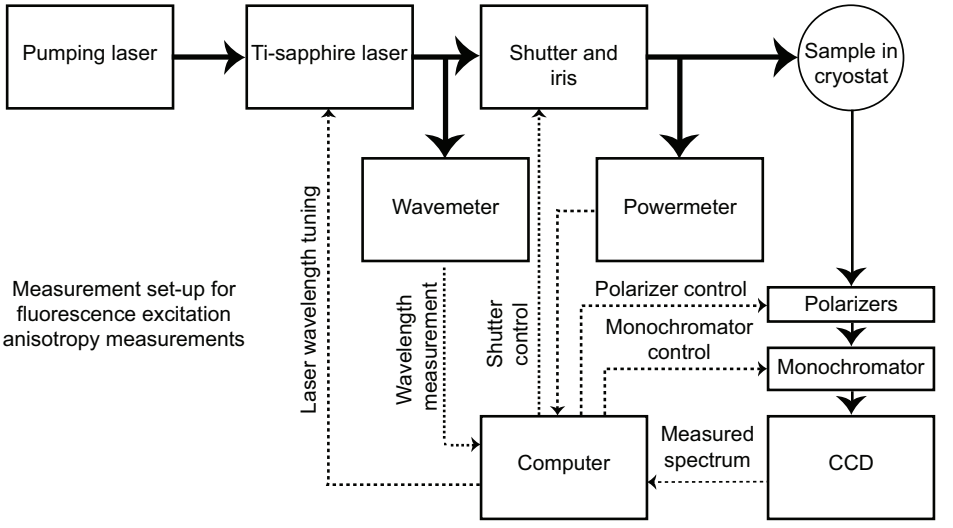

Figure 1.7. Fluorescence excitation anisotropy set-up. Solid lines show exciting laser (wider) and fluorescence signal (narrow). Dotted lines are measurement and control signals.

An important improvement in this set-up was addition of the powermeter to measure the intensity of exciting laser during the measurement continuously. This allowed to determine the average excitation intensity during each individual fluorescence measurement and therefore to correct the effect of laser intensity fluctuations to the measured anisotropy spectra.

1.4.4 Single-complex spectroscopy

In order to analyse the LH2 complexes in greater detail, we used single-complex spectra measured in cooperation with the group of Prof. J. Köhler (Bayreuth University, Germany) [88–91]. This set of data was instrumental do determine the behaviour of individual complexes.

For single-complex measurements, very low concentration samples of the complexes in solid poly vinyl alcohol (PVA) were made. Solid PVA has been determined to resemble the natural environment of the LH complexes [106,107]. Due to the low concentration, well separated single LH2 complexes were visible after excitation and fluorescence signal could be measured from those.

This dataset contained both fluorescence excitation spectra (summed over a long time period of about 60 minutes) and a large number of short-time exposures of fluorescence (a few seconds) from the same complexes. This allowed to differentiate between shorter and longer timescale processes, including static differences between complexes.

2 OBJECTIVES AND PRIMARY PROPOSITIONS

The main aim of this work was to experimentally study the robustness of excitons in samples of LH complexes against the complex structural and dynamic environments characteristic to biological systems, and to find adequate theoretical tools to describe these situations.

Within this agenda, the specific objectives of this work were:

- To investigate how the exciton zone evolves in different LH complexes along with increasing structural complexity and rising temperature.
- To find signatures of excitons in complete photosynthetic bacterial cells at physiological conditions.
- To develop a theoretical model for describing the localized photosynthetic exciton system that would be compatible with both single-molecule and ensemble spectroscopy experiments (including difference fluorescence line-narrowing and fluorescence excitation anisotropy data).
- To investigate the presence and extent of photosynthetic exciton self-trapping.

Primary propositions:

- Excitons are extremely resilient to the disorder in their surrounding environment, being present even in complete bacterial cells at temperatures of their native habitats.
- The exciton polaron model, complete with energetic and structural disorder, is able to model the spectral behaviour of LH2 complexes to a sufficient detail.

This work thus combines theoretical modelling and experimental measurements, as both were needed to reach the objectives.

3 DEVELOPMENT OF THE THEORETICAL MODEL

In theoretical analysis, we focused only on the LH2 complex from *Rps. acidophila*, although in experiments we studied a larger set of different samples, including photosynthetic antenna complexes from bacteria and even some simpler molecules relevant to photosynthesis, such as chlorin. The results from theoretical modeling of *Rps. acidophila* were used to qualitatively interpret spectra from other LH complexes as well. This chapter follows the models developed during the work, and to a certain extent, represents the evolution of our theoretical understanding of excitations in cyclic photosynthetic LH complexes from purple bacteria.

Following Silbey *et al* [83], we divided the theoretical studies into two stages, separating the calculations of excitonic interactions and excitonic lineshapes:

1. Determining the wavefunctions and excitation energies of the exciton states, which includes:
   a. Calculating the coupling matrix using dipole-dipole approximation, subsequently adding disorder.
   b. Finding the eigenstates of the Hamiltonian of the system.
2. Dressing the excitonic states with lineshapes:
   a. Calculating the spectral lineshapes according to exciton state energies and Huang-Rhys factors.
   b. Simulating absorption, fluorescence, and fluorescence excitation anisotropy spectra based on the lineshapes.

Although everything could have been modeled using a single Hamiltonian, this modeling workflow makes it easier to integrate experiments and theory and also provides more intuitive results by separating the excitonic structure and the spectroscopic effects through which it is studied. As an added benefit, separating the analysis of phonon sidebands is orders of magnitude quicker to calculate.

In this chapter, we give a brief overview of the theoretical modeling approaches used in the papers in a unified notation, putting the theoretical framework developed into a self-consistent form. The actual calculations were performed using MathCAD (mainly version 15) software from Parametric Technology Corporation by writing a series of programs based on the equations given in this chapter.

3.1 Excitonic model (Papers II and V)

3.1.1 Hamiltonians

The B850 ring contains 18 BChl a molecules, Q_y bands of which are excitonically coupled. Here, we consider the excitons to self-trap and form self-trapped excitons (STE) due to the experimentally observed strong coupling between the B850 exciton states and the phonons of the surrounding [42,44–46,108]. General theory of exciton self-trapping is, for example, provided in [23]. We have applied both Holstein [109] and Su-Schrieffer-Heeger [110] Hamiltonians in order to model these STEs.

Both of these are expansions of the rigid-lattice Hamiltonian [13]:

$$H_0 = \sum_n \left(\varepsilon_n + \delta\varepsilon_n\right)\left|n\right\rangle\left\langle n\right| + \sum_{n,m;n\neq m}\left(t_{nm} + \delta t_{nm}\right)\left|n\right\rangle\left\langle m\right|, \tag{3.1}$$

where ε_n are site excitation energies of the pigments (these would be the possible excitation energies in the complex if there was no excitonic coupling), $\delta\varepsilon_n$ are disorder realizations on the site-energy level, t_{nm} are coupling energies between the pigments n and m, and δt_{nm} are disorders in these couplings. In an ordered state, due to the structural dimerization of the B850 ring described in part 1.3, we consider the site excitation energies to be $\varepsilon_{2n} = \nu + \Delta/2$ and $\varepsilon_{2n+1} = \nu - \Delta/2$, for the α- and β-coordinated pigments, respectively. In this approach, the α- and β-coordinated site excitation energies differ by a constant value Δ, which according to our latest modeling is around 100 cm^{-1} (in literature, values from 0 to 532 cm^{-1} [16,52,54,58,59] have been proposed). The disorder model is discussed in the next sub-section.

The couplings t_{nm} were calculated according to the dipole-dipole approximation, as in [83], based on the structural model (see Fig. 3.1, also from [83], originally from [37]).

This structural model allows us to calculate the transition dipoles μ_n:

$$\begin{aligned}\mu_{2n} &= \begin{pmatrix}\sin\theta\cos\left(2\pi n/9 - \nu + \varphi_\alpha\right)\\ \sin\theta\sin\left(2\pi n/9 - \nu + \varphi_\alpha\right)\\ \cos\theta_\alpha\end{pmatrix}\\ \mu_{2n+1} &= \begin{pmatrix}\sin\theta\cos\left(2\pi n/9 + \nu + \varphi_\beta\right)\\ \sin\theta\sin\left(2\pi n/9 + \nu + \varphi_\beta\right)\\ \cos\theta_\beta\end{pmatrix}\end{aligned} \tag{3.2}$$

and their spatial locations:

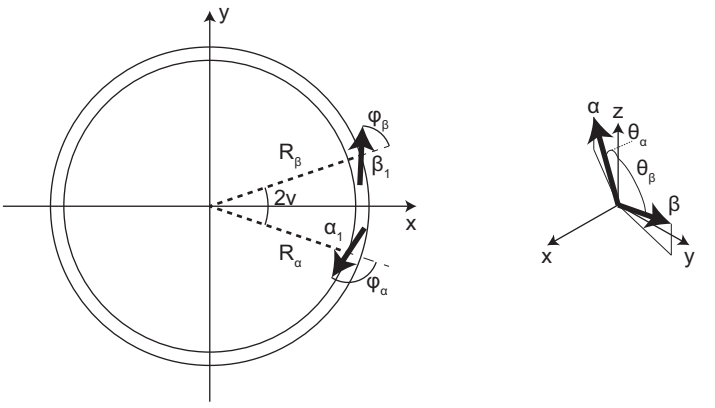

Figure 3.1. Simplified structural model of the B850 ring used in the calculations. The geometry for the two Q_y transition dipoles (black bold arrows) for pigments α_1 and β_1, constituting a dimeric sub-unit of the B850 ring, is shown in Cartesian coordinates. *R* denotes the distances of the pigments from the symmetry centre, and φ, θ and ν are structural angles for the corresponding pigments (denoted by subscript, if present). The B850 ring is formed when the dimeric subunit is repeated 9 times symmetrically. The original parameters were taken from [83]: $R_\alpha = 26.0$ Å, $R_\beta = 27.2$ Å, $\theta_\alpha = \theta_\beta = 84.9°$, $\nu = 10.3°$, $\varphi_\alpha = -112.5°$, and $\varphi_\beta = 63.2°$. In Paper II, we optimized all of them in a couple of percent range, in Paper VI, we only optimized the distances of the pigments from the symmetry centre.

$$r_{2n} = R_\alpha \begin{pmatrix} \cos(2\pi n/9 - \nu) \\ \sin(2\pi n/9 - \nu) \\ 0 \end{pmatrix} \quad . \qquad (3.3)$$
$$r_{2n+1} = R_\beta \begin{pmatrix} \cos(2\pi n/9 + \nu) \\ \sin(2\pi n/9 + \nu) \\ 0 \end{pmatrix}$$

The transition dipoles were used to calculate the couplings using dipole-dipole interaction model:

$$t_{nm} = B \frac{\mu_n \mu_m - 3\dfrac{(\mu_n L_{nm})(\mu_m L_{nm})}{L_{nm} L_{nm}}}{|L_{nm}|^3}. \qquad (3.4)$$

In equation (3.4), $L_{nm} = r_n - r_m$ are separation vectors (vectors connecting point-dipoles *n* and *m*) and $B = 1.895 \times 10^5$ cm^{-1} Å^3 [83].

When considering the structural parameters, it is important to note that optical spectra are more sensitive to the structural parameters than is the

resolution of crystal structures. This justifies adjustments of the crystal structure parameters by fitting to the optical spectral data. In Paper II, we successfully modelled the changes in the spectral properties by simulating thermal expansion of the complex.

In Paper II, following the track set in Refs. [45,46,111] (reviewed in [16]), we started the work with a model, according to which the excitonic states that absorb photons are regular rigid lattice (Frenkel) excitons [64] and the emitting states are the Su-Schrieffer-Heeger (SSH) excitons [110]. The absorbing states would be then described by the Hamiltonian (3.1) and the emitting states by

$$H = H_0 + c\sum_n (q_n - q_{n-1})\left(|n\rangle\langle n+1| + |n+1\rangle\langle n|\right) + \frac{1}{2}\sum_n (q_n - q_{n-1})^2. \quad (3.5)$$

In this equation, c is a coupling constant determining the strength of the exciton-phonon coupling leading to the self trapping of the exciton and q_n are the optimal distortions due to self-trapping (modifications to the side diagonal elements of the coupling matrix).

Later (Paper VI), in order to be consistent with the observations from line-narrowing spectroscopy [100], we advanced by enforcing the lowest-energy absorbing and emitting states to be resonant. The previous models referred to above, including the model of Paper II, allowed an energetic split between the $k = 0$ emitting states. In the updated model, we used the Holstein Hamiltonian [109] for both the absorbing and emitting states:

$$H = H_0 + c\sum_n q_n |n\rangle\langle n| + \frac{1}{2}\sum_n {q_n}^2. \quad (3.6)$$

The main difference between the two Hamiltonians is whether the diagonal or the off-diagonal elements of the coupling matrix are modified due to self-trapping (Holstein and SSH Hamiltonians, respectively). The practical reason for using the Holstein Hamiltonian was its physical transparency and better compatibility with the previous research [16] done in our laboratory. We found no qualitative difference in fitting the LH2 data with either the Holstein or the SSH Hamiltonian (except for a small change in the fitted parameters).

The eigenstates (eigenenergies E_k and eigenfunctions a_{nk}) of the excitonic or STE states were found through solving the eigenvalue problem:

$$\sum_m \langle n|H|m\rangle a_{mk} = E_k a_{nk} \quad (3.7)$$

In the case of the rigid-lattice Hamiltonian, the situation is simple; the result can be straightforwardly found as eigenvectors and eigenvalues of the coupling matrix. In the case of the Holstein and SSH Hamiltonians, however, the

situation is more complex and the eigenstates have to be found through an iterative optimization procedure [112], which also calculates the optimal distortions, q_n.

3.1.2 Model of disorder

In reality, all the complexes are different from each other. The differences can be modeled as disorder in the rigid-lattice Hamiltonian ($\delta\varepsilon$ and δt in (3.1)). Two forms of disorder have generally been introduced: internal and external, or intra-complex and inter-complex, respectively [113,114]. In this work, the intra-complex disorder signifies rearrangements taking place in a single complex in the course of the experimental time and the inter-complex disorder signifies differences in the environment around the complex or other differences that cause variations in the optical spectra that differ from complex to complex (see Fig. 3.2).

We analyzed the complexes through Monte-Carlo modeling, i.e. generating a large number of disorder realization and calculating the resulting spectra by summing over their contributions.

As it has been proven [115] that diagonal and off-diagonal disorders are practically indistinguishable, we used only diagonal disorder to simultaneously account for both the site energy and coupling disorders. This also means that structural disorder has been modeled by energetic disorder.

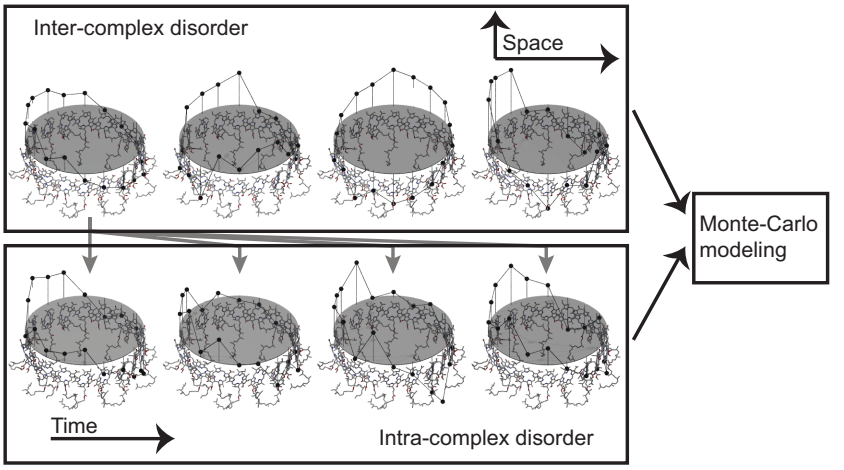

Figure 3.2. Intra-complex and inter-complex disorders (Paper VI). Diagonal site energy disorder $\delta\varepsilon$ is shown as a circular plot in relation to the grey circle, which signifies the level of zero disorder. The inter-complex disorder differs from complex to complex and makes the spectra collected from all complexes over time different. At the same time, each complex is also changing in time, leading to the intra-complex disorder. Both of these disorders account for the overall spectral characteristics and are taken into account in the Monte-Carlo modelling.

We started in Paper II [64] with a simple Gaussian disorder model, widely used in case of these complexes [16,51,83,111], which modulates the diagonal elements for internal disorder:

$$P(\delta\varepsilon) = \frac{1}{\sqrt{2\pi\sigma^2}} \exp\left(-\frac{\delta\varepsilon^2}{2\sigma^2} \right). \tag{3.8}$$

For the external disorder we used a Gaussian distribution of energy shifts (effectively changing all diagonal elements simultaneously by the same amount). This approach gave a large advantage in modeling, since the final absorption and fluorescence spectra could be just convoluted with this Gaussian, allowing to model the complex with a smaller number of disorder realizations.

This disorder model performed very well when studying only ensembles and produced excellent fits in our early works [64]. It later turned out that this simple model is not sufficient to explain the more subtle effects revealed by single-complex spectroscopy [88–91], such as splitting of the B850 band. There also had been reports that at least in some cases the LH2 complexes are disordered in a more correlated way, leading to elliptic disorder models [60–63].

Furthermore, single-complex spectroscopy (Paper VI) revealed how the disorder has to be divided into intra- and intercomplex parts (see Fig. 3.2). The intra-complex disorder we still considered to be distributed along a simple Gaussian, but for the inter-complex disorder we used a more elaborate model, which includes an elliptical modulation of site energies (originating from [60]):

$$\begin{aligned}
\delta\varepsilon^{\text{inter}}{}_{2n} &= \delta\varepsilon u_{2n} + \delta\varepsilon shift + \xi_1 \cos\left(2n\frac{\pi}{9} + \varphi_{1\alpha} \right) + \xi_2 \cos\left(4n\frac{\pi}{9} + \varphi_{2\alpha} \right) \\
\delta\varepsilon^{\text{inter}}{}_{2n+1} &= \delta\varepsilon u_{2n+1} + \delta\varepsilon shift + \xi_1 \cos\left(2n\frac{\pi}{9} + \varphi_{1\beta} \right) + \xi_2 \cos\left(4n\frac{\pi}{9} + \varphi_{2\beta} \right)
\end{aligned} \tag{3.9}$$

In (3.9), $\delta\varepsilon u$ is the uncorrelated Gaussian disorder, identical in application with the intra-complex disorder, but has a different standard deviation. $\Delta\varepsilon shift$ is the external correlated Gaussian disorder, as in Paper II. The latter two terms of (3.9) signify elliptical disorder: ξ_1 and ξ_2 are the weighs of the two components of disorder, sampled from Gaussian distributions. $\varphi_{1\alpha}$, $\varphi_{2\alpha}$, $\varphi_{1\beta}$ and $\varphi_{1\beta}$ are the phase noise, sampled from a uniform distribution. This allowed to model the complex fully, leading to the results of Paper VI, where we managed to determine the magnitudes of the intra-complex and inter-complex disorder parts.

It is important to stress here that the new disorder model contains two separate uncorrelated Gaussian disorders, both of which are needed to explain the single-complex measurements, while in ensemble experiment it is possible to use a single uncorrelated Gaussian disorder mode to account for all of the observed spectral effects.

3.2 Lineshape model (Papers I and IV)

3.2.1 General theory on simulation of fluorescence and absorption lineshapes of single states

An important part of this work was the study of spectral lineshapes consisting of the zero-phonon line (ZPL) and the phonon sideband (PSB) [64,104]. We have used several different lineshape models. The differences come from the spectral density function (SDF) of phonons and the way the resulting spectrum is calculated from it. Here we use the definition of phonon SDF at 0 K, $J(\omega)$, so that its integral is the Huang-Rhys factor [103] (also called the S-factor, S), i.e. the mean number of phonons involved in an optical transition. The integral of $\omega J(\omega)$ is the reorganization energy (λ) [81,116]:

$$\lambda = \int_{-\infty}^{\infty} \omega J(\omega) d\omega \tag{3.10}$$

$$S = \int_{-\infty}^{\infty} J(\omega) d\omega. \tag{3.11}$$

This model is valid only for very low temperatures; when the temperature is increased, the phonon bath also changes its nature, arriving to the definition of temperature-dependent phonon SDF.

$$\lambda(T) = \int_{-\infty}^{\infty} \omega J(\omega, T) d\omega. \tag{3.12}$$

$$S(T) = \int_{-\infty}^{\infty} J(\omega, T) d\omega. \tag{3.13}$$

The temperature-dependent SDF can be found from the 0 K SDF through the Bose-Einstein distribution as [73,81,103]:

$$J(\omega, T) = (1 + n(\omega, T)) J(\omega) + n(-\omega, T) J(-\omega), \tag{3.14}$$

where

$$n(\omega, T) = \frac{1}{e^{\frac{\hbar\omega}{k_B T}} - 1}. \tag{3.15}$$

From this general form, it is possible to calculate the emission spectrum of a pigment as [81]:

$$I(\omega)=\frac{1}{2\pi}\int_{-\infty}^{\infty}dt\exp(-i\omega t)\exp(G(t)-G(0)) \tag{3.16}$$

$$G(t)=\int_{-\infty}^{\infty}d\omega J(\omega,T)e^{-i\omega t} \tag{3.17}$$

The Taylor expansion of this is the equation more common for analysing the experimental fluorescence line-narrowing spectra [116,117]:

$$I(\omega)=\sum_{n=0}^{\infty}\frac{S(T)^n e^{-S(T)}}{n!}J_n(\omega,T). \tag{3.18}$$

In equation (3.18), $J_n(\omega,T)$ is the nth convolution of $J(\omega,T)/S(T)$ with itself. The $n = 0$ component corresponds to the ZPL, while the higher-order components form the PSB. The actual modeling was done over the equation (3.16), as described in [118], since it is much less computationally expensive, but mathematically equivalent. The computational speedup comes from the fact that the generator function can be used in conjunction with the Fast Fourier Transform (FFT). Also, this approach does not need the sum over components as in equation (3.18), leaving no possibility of artefacts due to not taking enough PSB components into account (effectively an infinite number of components is calculated).

In Paper IV, we studied the thermal evolution of phonon sidebands, and the model proposed here applied both in the case of chlorin and FMO [119] up until the highest temperatures experimentally measurable by difference fluorescence line-narrowing.

The equation (3.18) also leads to a convenient method for determining Huang-Rhys factors from the integrated intensities of the ZPL and the PSB.

$$\begin{aligned}\frac{I_{ZPL}}{I_{PSB}+I_{ZPL}}&=\frac{\int_{-\infty}^{\infty}\sum_{n=0}^{0}\frac{S(T)^n e^{-S(T)}}{n!}J_n(\omega,T)d\omega}{\int_{-\infty}^{\infty}\sum_{n=0}^{0}\frac{S(T)^n e^{-S(T)}}{n!}J_n(\omega,T)d\omega+\int_{-\infty}^{\infty}\sum_{n=1}^{\infty}\frac{S(T)^n e^{-S(T)}}{n!}J_n(\omega,T)d\omega}=\\ &=\frac{\sum_{n=0}^{0}\frac{S(T)^n e^{-S(T)}}{n!}\int_{-\infty}^{\infty}J_n(\omega,T)d\omega}{\sum_{n=0}^{0}\frac{S(T)^n e^{-S(T)}}{n!}\int_{-\infty}^{\infty}J_n(\omega,T)d\omega+\sum_{n=1}^{\infty}\frac{S(T)^n e^{-S(T)}}{n!}\int_{-\infty}^{\infty}J_n(\omega,T)d\omega}=\\ &=\frac{\sum_{n=0}^{0}\frac{S(T)^n e^{-S(T)}}{n!}}{\sum_{n=0}^{0}\frac{S(T)^n e^{-S(T)}}{n!}+\sum_{n=1}^{\infty}\frac{S(T)^n e^{-S(T)}}{n!}}=\frac{e^{-S(T)}}{\sum_{n=0}^{\infty}\frac{S(T)^n e^{-S(T)}}{n!}}=\frac{1}{\sum_{n=0}^{\infty}\frac{S(T)^n}{n!}}=e^{-S(T)}\end{aligned} \tag{3.19}$$

3.2.2 The traditional Gauss-Lorentz form

Initially, in Paper I, we approximated the spectral lineshapes with an empirical Gauss-Lorentz SDF form [104,117,120–123]. This form was traditionally used in order to provide the normalized convolutions of $J(\omega)$ (i.e. $J_n(\omega,T)$) pseudo-analytically, without the need for numerical convolution:

$$J_R(\omega)=\frac{4}{R}\left(\pi\Gamma+\Delta\sqrt{\frac{\pi}{\ln(2)}}\right)^{-1}\begin{cases}\dfrac{1}{1+\left(\dfrac{2(\omega-R\omega_m)}{\Gamma R}\right)^2} \; if \;\; \omega > R\omega_m \\ \exp\left(-\dfrac{4\ln(2)(\omega-R\omega_m)^2}{R^2\Delta^2}\right) if \;\; \omega \le R\omega_m\end{cases} \tag{3.20}$$

In this equation, R is the order of phonon sideband component, Γ is the FWHM of the Lorentzian part and Δ the FWHM of the Gaussian Part. ω_m is the peak position of the phonon SDF.

The form (3.20) is intuitive; its use also simplifies the modelling algorithms (it does not require the involvement of the FFT). However, it is mathematically flawed, since it does not reduce to zero at zero phonon energy, continuing to negative-energy side at 0 K. Also, due to the Lorentzian part, the reorganization energy of this form is infinite, which is unphysical.

3.2.3 Exponential polynomial form

Subsequently, in [64,118], we used a more physically correct (but still empirical) SDF model, based on an exponential polynomial [83]:

$$J(\omega)=\begin{cases}\displaystyle\sum_n \omega^n \cdot \exp\left(-\frac{\omega}{\omega_{cn}}\right)\frac{S_n}{n!\cdot\omega_{cn}^{\;n+1}} \; if \;\; \omega > 0 \\ 0 \; otherwise\end{cases} . \tag{3.21}$$

In this equation, S_n is the Huang-Rhys factor of the component n and ω_{cn} is the characteristic frequency for that component (has no direct physical meaning).

This form (3.21) has a finite reorganization energy and its value is zero at 0 phonon energy (if $n > 0$); therefore, it is physically realistic. In Papers II, IV and V, we used two-component models. In paper VI, only one-component model was applied since signal-to-noise ratio for the single-complex data was too large to make fitting of more components justifiable. The good fit in paper VI might still indicate that the need for the multiple components in papers IV and V does not actually come from single-complex lineshapes; this might be the result of the unavoidable ensemble averaging present in the experimental method and the actual underlying SDF might be simpler.

4 MODELING OF THE EXPERIMENTALLY OBSERVED SPECTRA

4.1 Estimating parameters for lineshapes

Knowing the eigenstates of Frenkel, Holstein and SSH excitons allows us to model their spectral properties. For this, as mentioned in the lineshape modeling section, we mostly require the state excitation energies, Huang-Rhys factors, and transition dipole moments.

The exciton state energies are the eigenenergies of the Hamiltonian, E_k, and in experiment these can be determined as the positions of the ZPL.

The Huang-Rhys factors we consider to be the product of the site Huang-Rhys factor S and the participation ratio of the state, p_k.

$$S_k = S\sum_n \left|a_{nk}\right|^4 = S \cdot p_k \tag{4.1}$$

The applicability of this equation is clearly shown in Paper VI. Since $p_k < 1$, this means that the site Huang-Rhys factor has to be greater than the Huang-Rhys factor of any excitonic state. For LH2, for example, S of 8.4 has been proposed [121].

The last important parameter for simulations is the exciton transition dipole, D_k, which can be used to determine the intensities of absorption and emission spectra, as well as the polarizational properties for fluorescence excitation anisotropy measurements. This can be calculated from the transition dipoles of the individual sites:

$$D_k = \sum_n a_{nk}\mu_n \ . \tag{4.2}$$

4.2 Absorption and fluorescence

Evaluation of the absorption and fluorescence spectra is straightforward from the exciton state lineshapes, as introduced in previous sections. The absorption spectrum (4.3) of a pigment (or an ensemble) at frequency ω is the sum of the lineshapes $I\left(\omega - E_k\right)$ of all possible excitonic states at this specific frequency, scaled with the squares of their dipole moments. The lineshapes $I\left(\omega - E_k\right)$ are assumed to contain the right Huang-Rhys factor and other parameters, which have been omitted from the formula for simplicity. For correct absorption spectrum, the sum has to be multiplied by wavenumber.

$$A(\omega) \propto \sum_k \omega D_k^2 I(\omega - E_k). \tag{4.3}$$

The calculation of emission spectra follows the same procedure, but the states are additionally multiplied by the corresponding Boltzmann factors, which determine the likelihood of thermal occupation of higher exciton states. The importance of using higher excitonic states became apparent in Paper II [64], because they are instrumental in the formation of higher-temperature fluorescence spectra. The emission spectra are scaled by the cube of the wavenumber [124].

$$F(\omega) \propto \sum_k \exp\left(-\frac{E_k - E_0}{k_B T}\right) \omega^3 D_k^2 I(E_k - \omega) \tag{4.4}$$

The lifetime broadening of the upper exciton-polaron states (from $k = 1$ to $k = 17$) was taken into account by convoluting with a Lorentzian with the FWHM of 80 cm-1; lifetime of the $k = 0$ state is far too long to be involved in modeling [16,65,105,125]; the $k = 0$ ZPL was modeled as a delta function (within the resolution of the FFT).

The apparatus function was also taken into account, where needed. We used either Lorentzian, Gaussian or Voigt profiles (mainly Gaussians were used, Lorentzian parts were required only in some ΔFLN measurements).

4.3 Fluorescence excitation anisotropy

Calculation of the fluorescence excitation anisotropy spectrum is more involved. In general, the fluorescence excitation anisotropy spectrum $r(\omega)$ is a weighted average of the angles between the absorbing and emitting dipole moments for a given excitation wavelength [9]. It can be obtained experimentally by measuring the emission from a sample excited with a linearly polarized spectrally narrow light source (with the wavenumber ω) and recording integral emission through either a polarizer that is polarized in parallel to it (IF_{vv}) or perpendicular to it (IF_{vh}).

$$r(\omega) = \left\langle \frac{3\cos\alpha_k - 1}{5} \right\rangle_k = \frac{IF_{vv}(\omega) - IF_{vh}(\omega)}{IF_{vv}(\omega) + 2IF_{vh}(\omega)}. \tag{4.5}$$

The anisotropy equation shown in brackets equally holds for each single combination of absorbing and emitting STE states (enumerated with k and n, respectively):

$$r_{kn} = \frac{3\dfrac{\left|D_k^{absorbing} \cdot D_n^{emitting}\right|}{\left|D_k^{absorbing}\right|\left|D_n^{emitting}\right|} - 1}{5}. \tag{4.6}$$

As equations (4.5) and (4.6) have to be simultaneously correct for each individual exciton state, we can evaluate the fluorescence excitation spectra for both polarization combinations.

$$I_{vv}(\omega)=\sum_{k=1}^{N}\left[A_k(\omega)\sum_{n=1}^{N}(1+2r_{kn})D_n^{emitting\,2}\exp\left(-\frac{E_k^{emitting}-E_0^{emitting}}{k_B\cdot T}\right)\right] \tag{4.7}$$

$$I_{vh}(\omega)=\sum_{k=1}^{N}\left[A_k(\omega)\sum_{n=1}^{N}(1-r_{kn})D_n^{emitting\,2}\exp\left(-\frac{E_k^{emitting}-E_0^{emitting}}{k_B\cdot T}\right)\right] \tag{4.8}$$

The final fluorescence excitation spectra can be found by summing together all of the fluorescence excitation spectra; this means all of the exciting and emmiting pigment combinations of all of the complexes and realizations of disorder present. The final fluorescence excitation anisotropy spectrum can then be found using equation (4.5).

4.4 Fluorescence line-narrowing and difference fluorescence line-narrowing

Fluorescence line-narrowing (FLN) is a great tool for revealing the finer details of the emission spectra of inhomogeneously broadened ensembles. In the common approach to FLN [126], the spectral lineshapes of an ensemble of pigments are all considered identical and their ZPLs are distributed according to the inhomogeneous distribution function (IDF). In delocalized excitonic systems (such as B850 of LH2) the physical meaning of IDF changes: it should now be considered as the density of states for the $k = 0$ exciton states.

The regular, non-selectively excited, fluorescence spectrum of an ensemble is just the convolution of the spectral lineshape of the pigment (or the excitonic state) with the IDF $N(\omega)$ [117]:

$$F(\omega)=\sum_{R=0}^{\infty}\left(S^P\frac{e^{-S}}{P!}\right)\int N(\Omega-\omega_{\max})J_P(\Omega-\omega)d\Omega \tag{4.9}$$

Here, the $\omega_{\max}$ is the peak position of the IDF, the IDF itself is a Gaussian with a given FWHM.

The FLN spectrum is obtained if the sample is excited with a spectrally narrow laser (with the exciting wavenumber of ω_E). This takes into account the probability of certain pigments or states being excited due to their lineshapes and energetic positions [117].

$$FLN(\omega) = \sum_{R,P=0}^{\infty} S^R \frac{e^{-S}}{R!} S^P \frac{e^{-S}}{P!} \int N(\Omega - \omega_{\max}) J_R(\omega_E - \Omega) J_P(\Omega - \omega) d\Omega \quad (4.10)$$

When spectral hole-burning with a spectrally narrow light source with an excitation wavenumber of ω_B for a time period of τ is taken into account, the IDF is modified by the spectral lineshape to account for bleached-out pigments [117]:

$$N(\tau, \omega - \omega_{\max}) = N(\omega - \omega_{\max}) \exp\left[-\sigma I \Phi \tau \sum_{Q=0}^{\infty} S^Q \frac{e^{-S}}{Q!} J_Q(\omega_B - \Omega) \right], \quad (4.11)$$

where σ, I and Φ are the absorption cross-section, laser intensity and quantum yield, respectively.
From it, we can calculate the ΔFLN spectra for short burn time limit:

$$\Delta FLN(\omega) = \sum_{R,P,Q=0}^{\infty} S^R \frac{e^{-S}}{R!} S^P \frac{e^{-S}}{P!} S^Q \frac{e^{-S}}{Q!} \int N(\Omega - \omega_{\max}) J_Q(\omega_B - \Omega) J_R(\omega_E - \Omega) J_P(\Omega - \omega) d\Omega \quad (4.12)$$

These equations can be simplified by directly using the lineshape:

$$F(\omega) = \int N(\Omega - \omega_{\max}) I(\Omega - \omega) d\Omega \quad (4.13)$$

$$FLN(\omega) = \int N(\Omega - \omega_{\max}) I(\omega_E - \Omega) I(\Omega - \omega) d\Omega \quad (4.14)$$

$$\Delta FLN(\omega) = \int N(\Omega - \omega_{\max}) I(\omega_B - \Omega) I(\omega_E - \Omega) I(\Omega - \omega) d\Omega \quad (4.15)$$

The model can be further expanded to allow Monte Carlo modeling by replacing the general disorder distribution with the simulated distributions of the single complex realizations, each with their own $k = 0$ site energy and Huang-Rhys factor. This leads to a new set of equations (using δ instead of N to signify the treatment of realizations of complexes separately):

$$F(\omega) = \sum_n \int \delta(\Omega - E_n) I(\Omega - \omega) d\Omega = \sum_n I(E_n - \omega) \quad (4.16)$$

$$\begin{aligned} FLN(\omega) &= \sum_n \int \delta(\Omega - E_n) I(\omega_E - \Omega) I(\Omega - \omega) d\Omega = \\ &= \sum_n I(\omega_E - E_n) I(E_n - \omega) \end{aligned} \quad (4.17)$$

$$\Delta FLN(\omega) = \sum_n \int \delta(\Omega - E_n) I(\omega_B - \Omega) I(\omega_E - \Omega) I(\Omega - \omega) d\Omega = \\ = \sum_n I(\omega_B - E_n) I(\omega_E - E_n) I(E_n - \omega) \tag{4.18}$$

In these equations, n denotes the $k = 0$ states of different realizations of the LH2 complex. Mathematically, it would be useful to replace the delta function with the only energetically shifting inter-complex disorder, since it behaves identically to the IDF in equation (4.9) for each realization of the complexes. Due to time constraints this avenue was not explored enough to yield results, but will hopefully lead to results in the future.

5 EXCITATION WAVELENGTH DEPENDENT ELECTRON-PHONON COUPLING (PAPER I)

As understanding of spectral lineshapes and phonon sidebands is important for modelling all spectra, our work was started by studying phonon sidebands of simpler photosynthetic molecules, such as chlorin (7,8-dihydroporphin) and chlorophylls, and then continued to more complex light-harvesting systems, such as the FMO [119] and LH2 complexes. The chlorin research was expanded in Paper IV by updating the phonon spectral density function theory and confirming the applicability of the temperature dependency theory of the lineshape.

In Paper I [104] we studied the excitation wavelength dependence of the Huang-Rhys factors of emission spectra from low-temperature glasses containing chlorin and chlorophyll a by using the ΔFLN technique. For simpler molecules, such as chlorin, it is possible to measure the ΔFLN spectra over the whole IDF in the sample (see Fig. 5.1).

We analysed the spectra obtained from the ΔFLN experiments according to the theory section 3.3.4. The Huang-Rhys factors were first determined straight from the ΔFLN spectra (using equation (3.19)) and also from fitting the lineshape model to the experimental spectra (both results can be seen in Fig. 5.1). In this early work, we fitted the spectra based on the Gauss-Lorentz lineshape model, as described in the theory section. Convolutions were approximated by analytic means (also described in the theory section).

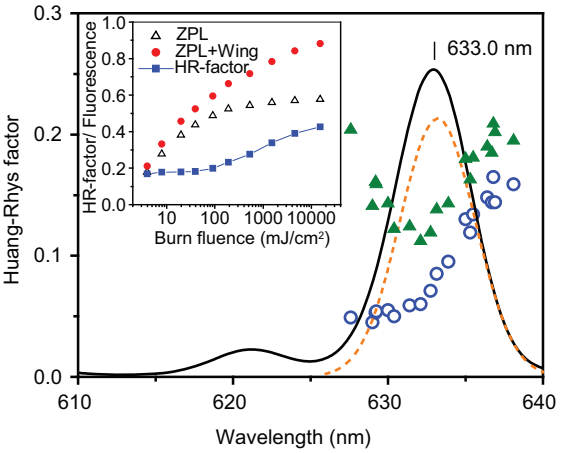

Figure 5.1. Dependence of the Huang-Rhys factor on the excitation wavelength [104]. The black line is the absorption spectrum of chlorin, dashed line the IDF, the triangles are the apparent Huang-Rhys factors and the circles the Huang-Rhys factors from fitting. The inset shows the dependence between burn fluence and observed Huang-Rhys factors, ZPL and PSB intensities.

Although we did not publish the results from this, the analysis of the data presented in this article was also in parallel performed using the exponential polynomial phonon spectral density function form and mathematically correct convolutions. This yielded very similar results, since the Huang-Rhys factors were small. Still, this shift in analysis paved the way for the following research papers. This eventually led to the adoption of the generator function approach that can be made fast enough using the Fast Fourier Transform to be able to perform extensive Monte-Carlo simulations in an acceptable timeframe.

The results showed that the Huang-Rhys factors increase with increasing wavelength (see Fig. 5.1) for the first time. The results for chlorin showed an increase of the PSB Huang-Rhys factor from 0.05 to 0.16 over ≈ 10 nm spectral range and from 0.17 to 0.49 for chlorophyll a (between 669.3 and 693.3 nm). This hints that similar behaviour might appear in the individual BChl a sites in LH complexes as well. However, the time allocated for the thesis work did not allow exploring this interesting aspect any further. We determined that the vibronic Huang-Rhys factors were relatively unaffected by the excitation wavelength. This latter issue has been in more detail analysed in paper V, see Chapter 9.

6 THE EVOLUTION OF EXCITONS IN LH2 COMPLEX FROM 4.5 K TO ROOM TEMPERATURE (PAPER II)

One main objection against the biological significance of excitons has been the high thermal noise present at physiological temperatures. Therefore, even if excitons can be proven to exist at the low temperature limit, this might be an artefact due to the abnormally low temperatures, being not relevant at physiological temperatures.

To explore this, we measured the absorption, fluorescence and fluorescence excitation anisotropy spectra of LH2 complexes from *Rps. acidophila* from 4.5 K to room temperature and analysed them using theoretical modelling [64].

The main indication for the presence of the excitonic zone is the two dips in the fluorescence excitation anisotropy spectrum. As can be seen from the experimental data in Fig. 6.1, at least the high-energy anisotropy dip around 765 nm can be clearly traced along the whole temperature range from 4.5 K to 263 K. This kind of a double-dip behaviour is also common for the LH1 complex, and not only in *Rps. acidophila* but in *Rb. sphaeroides* as well (see Paper III). So we set out to model the temperature dependence of the fluorescence excitation anisotropy, absorption and fluorescence spectra for LH2 complexes according to the theoretical model as described in the theoretical section.

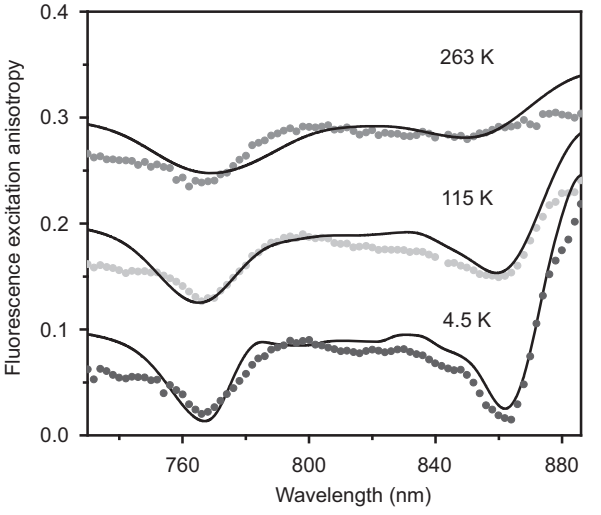

Figure 6.1. Measured and modelled fluorescence excitation anisotropies from 4.5 K to 263 K for LH2 complexes from *Rps. acidophila*. Measurements are indicated by symbols, the modelling results by continuous lines [64].

We analysed the spectra by using the model described in the theoretical model chapter 3.3.3. This time we considered the absorbing states to be Frenkel excitons [13] and emitting states STEs [23,44–46], described by the SSH Hamiltonian [110]. Also, in this work we used the modelling convention that the excitonic states are labelled from $k = 0$, $k = \pm 1$ to $k = \pm 8$ and $k = 9$. Later we abandoned this naming scheme due to the fact that the + and – have meanings as the directions of perpendicular dipole moments only in the case of perfectly ordered B850 state. In case of a disordered model, it is more natural to use simpler numbering from $k = 0$, $k = 1$ to $k = 16$ and $k = 17$, based solely on the energetic order of the states.

It can be seen in Fig. 6.2 that there is a good agreement between the modelling and the experiment. The B850 band positions shift to higher energies and they generally become wider, as also noted earlier [46,127–129]. To explain the behaviour, we used thermal expansion of the complex using an empirical sigmoid function (average distance between the pigments increases by about 0.05 nm from near absolute zero to room temperatures, in line with [36]). The choice of the sigmoidal function was justified by earlier research [130,131].

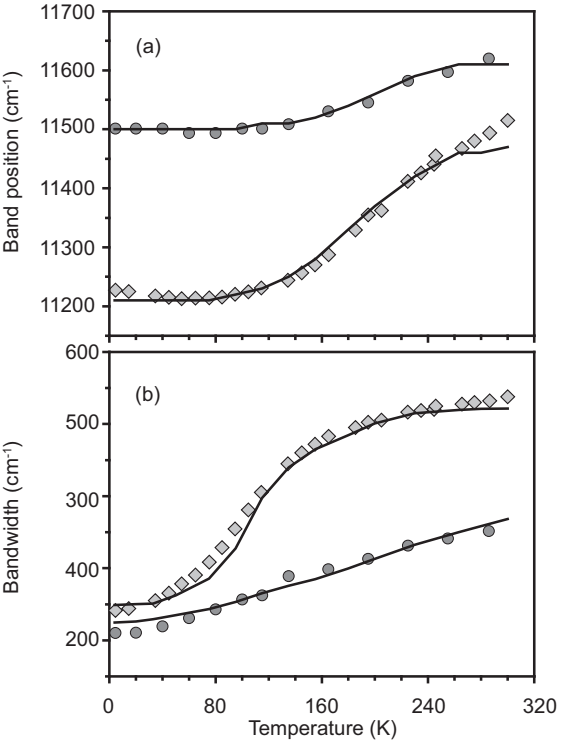

Figure 6.2. Temperature dependences of the B850 fluorescence (diamonds) and absorption (circles) band peak positions (pane a) and bandwidths (FWHM, pane b) of the LH2 complex from *Rps. acidophila*. The scattered points show measurements, solid lines model results [64].

It is also notable that the changes in the fluorescence spectra are much more prominent, hinting to different underlying processes. The more prominent changes in the emission spectra were determined to be due to thermally assisted occupation of higher STE levels (primarily ±1, see Fig. 6.3), which we modelled using Boltzmann factors as in equation 4.4.

The main result of this article, however, was the measurement and detailed modelling of the changes in the fluorescence excitation anisotropy spectra over the temperature range (see Figure 6.1, 6.3). The fluorescence excitation anisotropy had been earlier measured only at very low temperatures (close to 4.5 K). From the experimental spectra it became apparent that the high-energy anisotropy dip does not change its shape or position considerably during the temperature range, paving the way to proving the presence of excitons in full cells at physiological conditions.

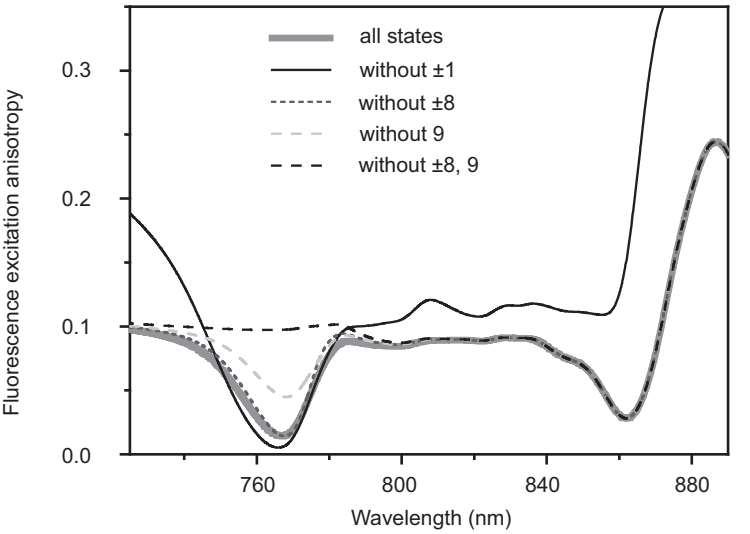

Figure 6.3. Formation of the anisotropy minima of the LH2 complex from *Rps. acidophila* at 4.5 K. Different lines show how the fluorescence excitation anisotropy spectrum would appear if some of the excitonic states are removed from calculations. Spectrum with all of the states present is shown for reference. It can be seen that the low-energy (high-wavelength) dip is caused mostly by the ±1 states, while the high-wavelength dip is caused by a combination of ±8 and 9 [64].

The other important result was determination of the correspondence between the excitonic states and their respective features in the anisotropy spectra (see Fig. 6.3). As it had been predicted earlier, the low energy dip is mostly due to the $k = 1$ and $k = 2$ states. The $k = 1$ state is closer in its orientation to the $k = 0$ state and $k = 2$ state is on average perpendicular to it [16]. So, the two lowest-energy states cause the anisotropy rise on the low-energy side and the third state forces anisotropy lower, causing the high-wavelength dip in the region, where $k = 2$ absorption overpowers $k = 1$ absorption (therefore, the anisotropy dip is also shifted from the B850 maximum). Interestingly, the nature of the high-wavelength dip is more complex: it forms in combination of ±8 and 9 states. All in all, the correspondence between the exciton states and anisotropy features justifies the estimation of exciton zone widths solely from the anisotropy spectra, which we used heavily in paper III.

7 EXCITONS AT PHYSIOLOGICAL TEMPERATURES IN A BACTERIAL CELL (PAPER III)

Next, we moved on to one of the primary purposes of the thesis, proving that the excitons are really present in living cells. There had been no concrete evidence of the excitonic structure within the LH2 complex in living cells before and the biological significance was extrapolated from the conditions at very low temperatures, based on the behaviour of the absorption, emission and circular dichroism spectra.

In the work, we studied the spectral features of different light-harvesting complexes systematically by moving from the low-temperature domain to room temperature, while increasing the complexity of samples.

Our samples in this study were from *Rb. sphaeroides*: isolated and membrane bound LH2 and RC-LH1-PufX complexes, full photosynthetic membranes and the living cells. From the absorption spectra (Fig. 7.1.), it is visible that the spectral characteristics of the photosynthetic membranes and the cells remind the sum of spectral characteristics of the LH2 and RC-LH1-PufX complexes.

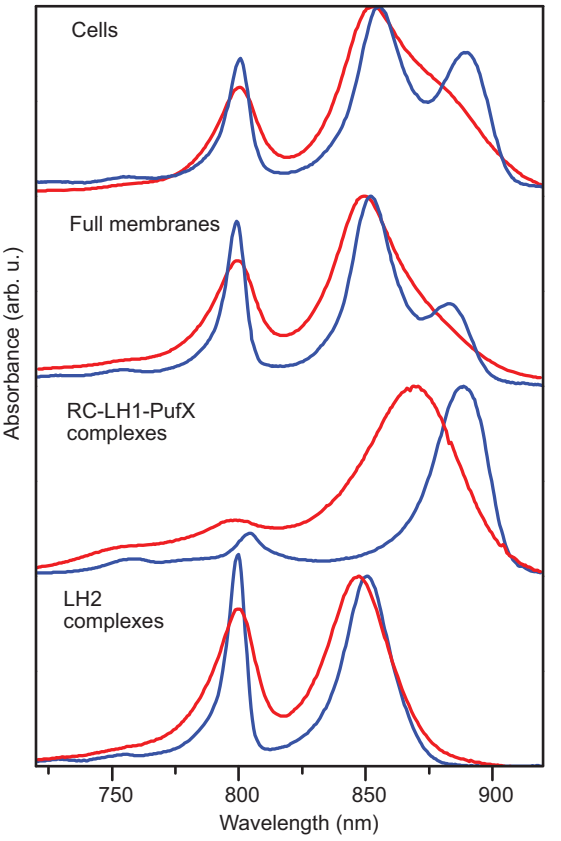

Figure 7.1. Absorption spectra of the *Rb. sphaeroides* samples studied at 4.5 K (blue) and room temperature (red). The order of complexity increases from the isolated LH2 complexes at the bottom to the full cells at the top. It can be seen that the spectral features of the LH complexes survive the integration into more complex levels [25].

To move on with the task of proving the presence of excitons in the complete cells, we started studying the fluorescence excitation anisotropy spectra, as the dips are clearly correlated with the border states of the excitonic manifold, as was shown in Paper II. Our earlier measurements also gave us confidence to find at least the high-energy anisotropy dip at room temperature.

To approach the problem systematically, we started by measuring the LH2 and RC-LH1-PufX complexes at 4.5 K separately, and detected the presence and position of the two anisotropy minima (see Fig. 7.2.). We also increased the temperature from 4.5 K to room temperature and observed that the minima remained [25].

To move on, we measured the fluorescence excitation anisotropy of full membranes at 4.5 K and room temperature. It can be seen from Fig. 7.2 that the anisotropy minima are exactly where they have been expected to appear from the spectra of isolated complexes. When the temperature was increased, the high-energy minimum remained, but the low-energy minima almost disappeared.

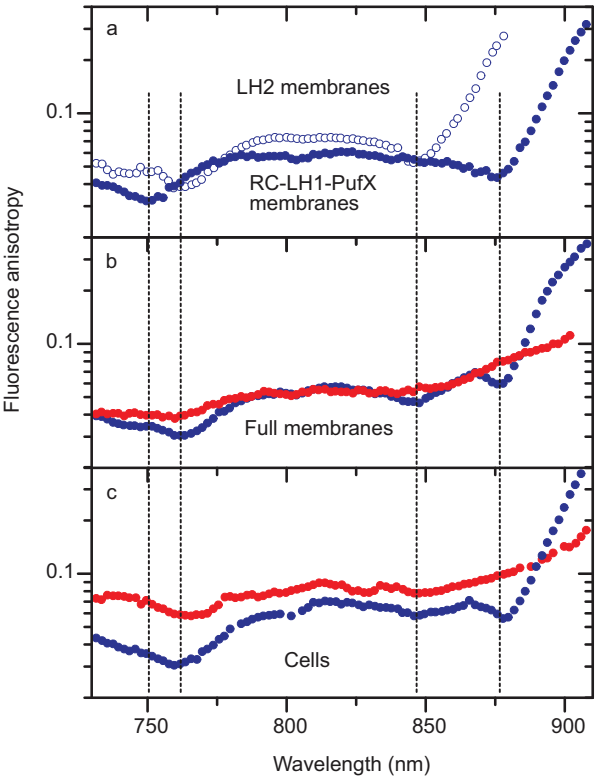

Figure 7.2. Tracking the evolution of fluorescence excitation anisotropy spectra from 4.5 K to room temperature (blue and red, respectively), and from isolated complexes to full *Rb. sphaeroides* cells. a) Anisotropy spectra of isolated LH2 and RC-LH1-PufX complexes at 4.5 K. b) The low-temperature and high-temperature spectra for full membranes. c) Spectra from complete cells [25].

For finalizing the experiments, we measured the anisotropy spectra in complete *Rb. sphaeroides* cells, which showed similar behaviour: at the low-temperature limit both minima are clearly visible, but when temperature in increased, only the high-energy dip remains. Still, there are residues of the LH2 low-energy wavelength dip. This proved that excitons are indeed relevant in physiological conditions and therefore an irrefutable link with biology was established.

In the same paper, we also estimated the exciton zone widths (inter-minimum distances in fluorescence excitation anisotropy spectra) for a large set of LH complexes from both *Rb. sphaeroides* and *Rps. acidophila* at 4.5 K (see Table 1). The results show that the exciton zone is systematically wider in the case of membrane samples, possibly showing that they are a more suitable environment for excitons, compared to detergent-isolated samples. This shows that the unnatural conditions present in experiment might actually work against excitonic interaction (not amplify it as an artefact). Still, the natural configuration of LH1, the RC-LH1-PufX complex, has the smallest exciton zone width of LH1 configurations studied (but the difference is marginal).

Table 7.1. Bandwidths of excitons in detergent-isolated and membrane-embedded light-harvesting complexes from *Rb. sphaeroides* and *Rps. acidophila* at 4.5 K. [25]

Sample			Dips in the spectrum (±0.5 nm)		Bandwidth a) (±15 cm^{-1})
			High-energy	Low-energy	
Rps. acidophila	LH2	complex	766.5	861.7	1442(13)
		membrane b)	765.8	863.1	1473(27)
	LH1	membrane b)	765.6	901.6	1969(15)
Rb. sphaeroides	LH2	complex	762.1	841.6	1241(16)
		membrane	763.2	845.8	1279(9)
	LH1 c)	complex	755.7	880.1	1871(3)
		membrane	749.6	882.8	2013(22)
	RC-LH1 c)	complex	751.8	880.1	1939(39)
		membrane	751.1	880.4	1955(20)
	RC-LH1-PufX	complex	749.8	873.3	1886(41)
		membrane	751.5	869.5	1892(22)

a) Defined as the energy difference between the high-energy dip of the polarized fluorescence excitation spectrum and the low energy dip

b) Obtained from full membrane's spectra by integrating only the corresponding (LH1 or LH2) emission regions.

c) From [105].

8 TEMPERATURE DEPENDENCE OF ELECTRON-PHONON COUPLING IN LOCALIZED OR WEAKLY EXCITONICALLY COUPLED SYSTEMS (PAPER IV)

To verify the phonon temperature dependency model, widely used in our modelling, we measured ΔFLN spectra as a function of temperature for chlorin, which represents a localized electronic system and FMO, a weakly excitonically coupled system [118].

The spectra were measured from 4.5 K to 69 K for chlorin and from 4.5 K to 51 K for FMO. Both sets of spectra were fitted with the lineshape model using the SDF defined at 0 K (the SDF itself was different for chlorin and FMO). The modelling was performed as described in the theory section. The results show that both complexes can be modelled using this method, although the fitting results for chlorin appear more precise. In case of the FMO, most likely the weak exciton interaction between the pigments is to blame for the mismatch [118].

The measured spectra alongside with the modelled spectra are on Fig. 8.1. Each pane shows also the modelled S factor for that complex at a certain temperature, based on the fitting.

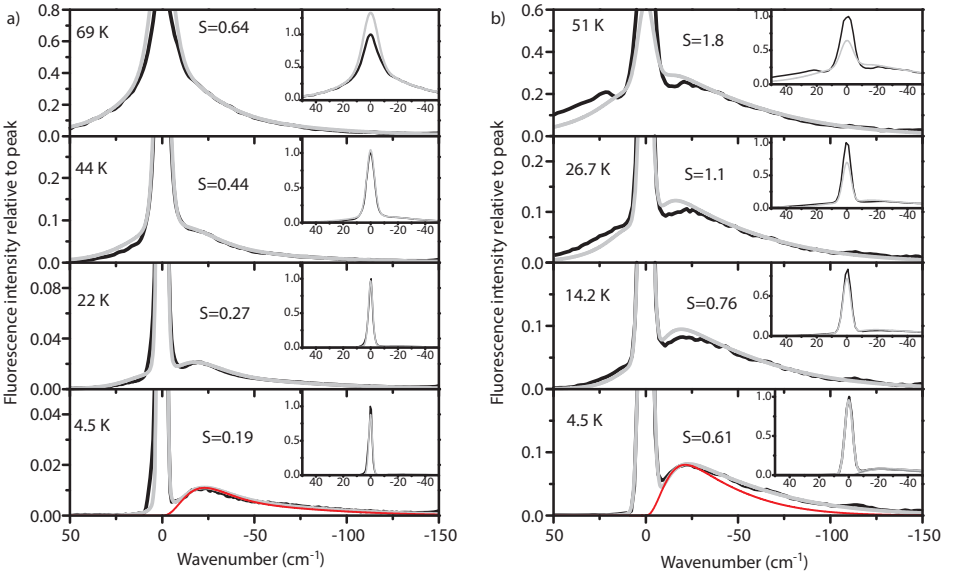

Figure 8.1. Temperature dependency of phonon sidebands for a) chlorin and b) FMO. Main graph areas show the homogeneous spectra, relative to the ZPL positions, enlarged to make the details in the phonon sideband noticeable. The insets show the ZPL region without cropping. Black lines show the experimental spectra, grey lines the fitted spectra. The thin red line in the 4.5 K spectrum is the phonon SDF [118].

The research also yielded interesting information about the temperature dependence of the ZPL width for chlorin (see Fig. 8.2). According to regression, the FWHM of the ZPL is proportional to $T^{2.2}$, implying that the system cannot be explained by a simple two-level model [132–136].

These data gave us some confidence that the lineshape model used in our earlier research is appropriate.

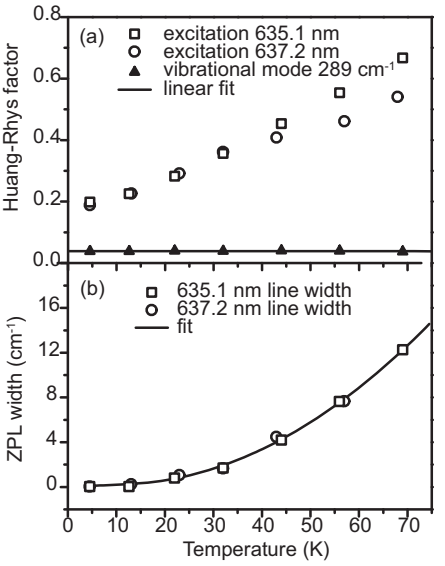

Figure 8.2. Temperature dependencies of the Huang-Rhys factor (a) and ZPL width (b) for the chlorin-doped propanol glass. In (a) the open symbols show how the phonon sideband Huang-Rhys factors depend on temperature for the two excitation wavelengths: 636.1 nm and 637.2 nm. Black triangles show the vibronic Huang-Rhys factor. In (b) the open symbols are again the ZPL widths for the two excitation wavelengths and the solid line is the fitted $T^{2.2}$ dependency [118].

9 MODIFICATIONS OF VIBRATIONAL AND PHONON COUPLINGS IN LIGHT-HARVESTING COMPLEXES (PAPER V)

In this work, both experimentally and theoretically, we investigated how the vibrational and phonon couplings for localized BChl a are modified when assembled in excitonically coupled LH complexes. Since the theoretical part concerning vibronic couplings was done by Dr. Juha Matti Linnanto, and is not included into this thesis, we will not discussed it in detail here (please refer to the Paper V).

As delocalization is known to lead to a decrease in the phonon couplings as per equation (4.1), it would be expected that both the phonon and vibrational couplings would decrease when the BChl a molecules are incorporated into the LH complexes. The effect of delocalization, for example, was used to successfully analyse the behaviour of Huang-Rhys factors in Papers II and VI.

Still, from earlier work it is known that in LH1 and LH2 complexes only vibrational couplings decrease (compared to isolated BChl a), while phonon couplings actually increase. For example, in the BChl a-doped triethylamine glass at 4.5 K the Huang-Rhys factor characterizing the total electron-phonon coupling strength, S_{ph}, is about 0.5 and the total vibronic coupling strength,

Table 9.1. Fluorescence spectral characteristics of BChl *a* in solid solution and in protein environment.

Sample	Excitation wavelength (nm)	FWHM of IDF (cm^{-1})	S_{ph}	S_{vib}	Reference [a]
BChl *a* in triethylamine	787.0	320±40	0.51±0.1	0.37±0.04	[137,138]
FMO complex (*Cb. tepidum*)	827.1	66±5	0.58±0.1	0.42±0.04	[101]
LH2 complex (*Rb. sphaeroides*)	870.5	147±10	2.0±0.2	0.09±0.01	[108] [b]
LH2 complex (*Rps. acidophila*)	891.0	120±10	2.3±0.2	0.09±0.01	[130] [b]
LH1 complex (*Rb. sphaeroides*)	900.1	119±10	1.8±0.2	0.09±0.01	[108] b)

[a] For comparability's sake, the *S*-factors obtained in previous publications have been re-scaled according to the experimental and calculation procedures taken in the present work.
[b] This work.

$S_{vib} \approx 0.4$ [137,139] (see Table 9.1). When the same pigments are inserted into the protein matrix of LH2, the vibronic coupling decreases about fourfold to 0.09, as expected. At the same time, the total phonon coupling increases practically fourfold, reaching 1.8 to 2.3 in the LH2 complexes from *Rps. acidophila* and *Rb. sphaeroides*. The aim of this work was to shed light on this counterintuitive behaviour.

Experimentally, we measured ΔFLN spectra of LH complexes (see Fig. 9.1) and determined both the phonon- and vibronic couplings, and FWHMs of the density of emitting states, i.e. the inhomogeneous distribution function (IDF).

At the same time, theoretical modelling of the vibrational interaction [140] was performed, which showed that within the complex delocalization decreases the S_{vib} Huang-Rhys factors. When disorder is applied, the excitons tend to localize more and therefore the Huang-Rhys factors increase. This agrees with the modelling in Papers II and VI.

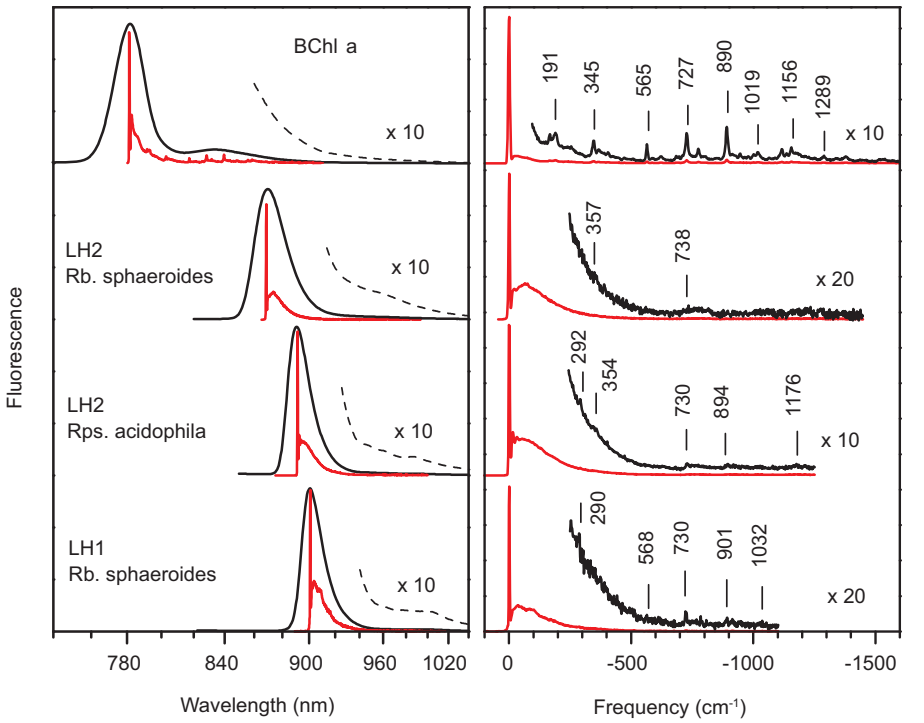

Figure 9.1. On the left panel, we show the comparison between the low-resolution (black line) and high-resolution (ΔFLN, red line) fluorescence spectra of BChl a in solid solution of triethylamine and in various LH protein complexes: LH1 and LH2 from Rb. sphaeroides, and LH2 from Rps. acidophila. The peak-normalized spectra were recorded at 4.5 K and are presented in reciprocal wavelength (energy) scale. Shown with dashed lines are the 10-fold amplified tails of the low-resolution spectra. (Right panel) Peak-normalized ΔFLN spectra of the same samples in relative wavenumber scale; vertical lines label selected vibrational mode frequencies [104].

To meet the experiment in case of LH1 and LH2 complexes, we concluded that the effective S_{ph} for the sites have to be very large, S = 8.8 according to Paper VI. Such large site phonon Huang-Rhys factors have also been proposed by others (S of 8.4 in [128]). One explanation for the unexpected large site phonon Huang-Rhys factors is that the applied model is not adequate. Another explanation, which we prefer, is that upon assembly into the LH complexes the nature of electronic states changes. For example, due to the involvement of charge-transfer states that can arise from the close proximity of BChl a molecules in the LH complex rings. The presence of CT states in LH1 and LH2 complexes is experimentally supported by observations of the electrochromic (Stark) effect [141,142] and high-pressure induced bandshifts [143], and theoretically, by quantum chemical calculations [53,80,82,144].

10. A UNIFIED STUDY OF SINGLE-COMPLEX AND ENSEMBLE DATA (PAPER VI)

During the final part of our studies we obtained a set of single-complex spectra of LH2 complexes from *Rps. acidophila* [88–91] in PVA (polyvinyl alcohol) at 1.2 K. PVA has been proven to be an excellent matrix to study the LH2 complexes in [106,107]. The dataset contained excitation spectra from 26 complexes, integrated over a long time period (a set of repetitions summed over about an hour) and a large number of fluorescence spectra (each exposure in the order of a couple of seconds). The fluorescence spectra from a single LH2 complex showed great variances, which gave us a direct method for studying the microscopic disorder in the complexes that would be averaged out in ensemble studies.

The excitation spectra and summed fluorescence spectra (the sum of all individual fluorescence spectra obtained from a single complex) for two example complexes can be seen in Fig. 10.1. From the data it was evident that the averaged excitation and emission spectra were different for each complex, leading to the adoption of the inter- and intra-complex disorder models, as described in more detail in the theory section. The inter-complex disorder causes the long-time average spectra of each complex to differ; the intra-complex disorder causes differences between single short integration time spectra obtained from a single complex.

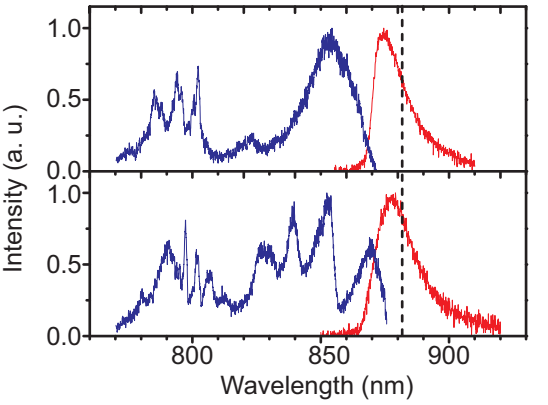

Figure 10.1. Two examples of single-molecule excitation and emission spectra, integrated over long time (about an hour for the excitation spectra and slightly less for the emission spectra). These correspond to two realizations of inter-complex disorder that have been summed over intra-complex disorder. The vertical line indicates the position of the maximum of the sum of all fluorescence spectra in figure 10.4.

To analyse the disorder models in greater detail, we attempted to extract as much information from the obtained single short-time fluorescence spectra as possible. As at the low temperature limit the LH2 complex emits almost solely from the $k = 0$ excitonic state, the emission spectra are the lineshapes of the lowest excitonic state and therefore we can use the spectra to determine the excitation energies and Huang-Rhys factors of the lowest excitonic state. To determine these, we developed a modified Levenberg-Marquardt [145] method to fit the lineshape model used to the single spectra. The results of this fitting in case of two individual spectra can be seen in Fig. 10.2. While the signal-to-noise ratio of single-complex fluorescence spectra is poor, it can be still seen that fitting can yield reasonable results.

The Huang-Rhys factors and ZPL positions obtained by fitting are shown in Fig. 10.3. It can be seen that the Huang-Rhys factors and ZPL positions vary between the individual spectra from a single LH2 complex and the point clouds corresponding to different complexes do not overlap completely, showing again the necessity to distinguish between intra- and inter-complex disorders. In this case the variance within the point cloud of a single complex is caused by intra-complex disorder, while the differences between the point clouds of different complexes are caused by the inter-complex disorder.

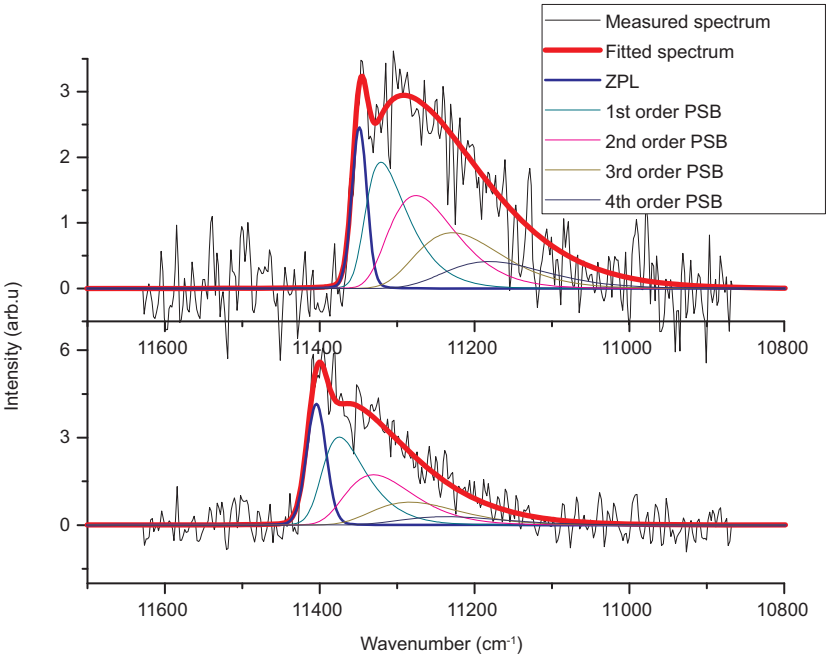

Figure 10.2. Fitting the spectrum of a single realization of an LH2 complex. The components are shown according to the equation (3.18). It can be seen that the signal-to-noise ratio of single-complex measurements is not very good, but a reasonable fit can be obtained.

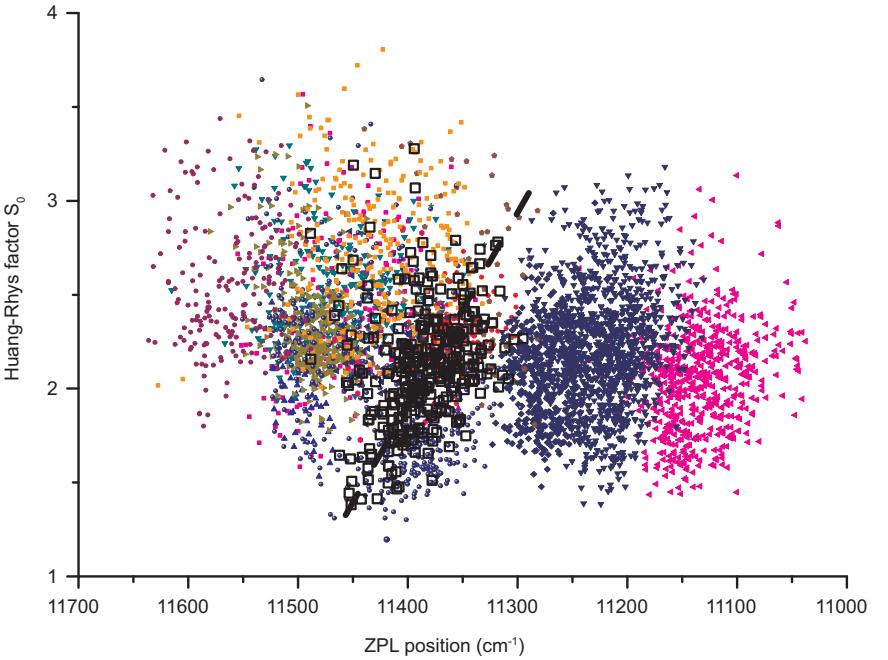

Figure 10.3. Fitting results of Huang-Rhys factors for single-complex spectra. Different colours and symbols denote different complexes. A point cloud corresponding to a single complex has been highlighted and a trendline, showing the dependence between the S_0 Huang-Rhys factors and the ZPL positions, has been added.

We suspected that the single-complex measurements were biased, i.e. the selection of complexes for measurement did not uniformly cover the full distribution present in a realistic sample. Therefore, to study the microscopic behaviour, we still had to rely on ensemble spectra to try to determine the realistic spectra.

The ensemble spectra for the complex, compared to the spectra obtained from the sum of all single-complex spectra, can be seen in Fig. 10.4. For the ensemble we have excitation, fluorescence and fluorescence excitation anisotropy spectra. It can be seen that the excitation spectrum of the ensemble is narrower than the summed excitation spectrum of single complexes, also the fluorescence spectra are more red-shifted in single-complex spectra. Based on this data, we set out to construct a theoretical model that would explain the characteristics of both ensemble and single-complex spectra while explaining the differences and sources for possible biasing in single-complex spectra.

The theoretical model used is described in detail in the theory section. In principle, we upgraded the disorder model from our previous works to account for the distribution of single-complex spectra, mainly by adding an elliptic disorder model [60].

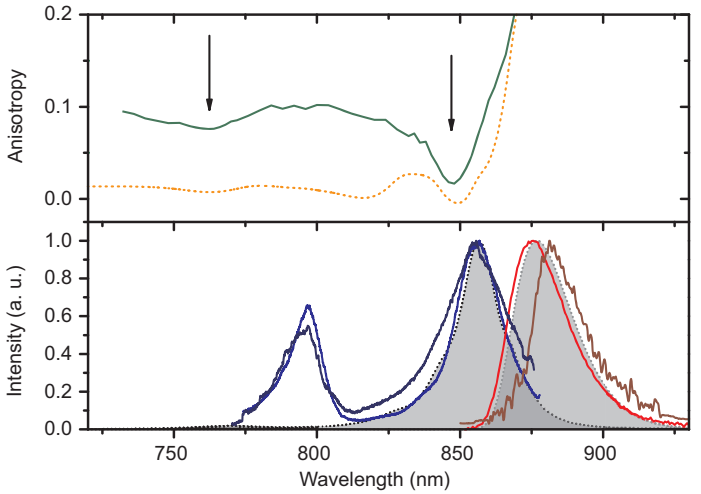

Figure 10.4. Comparison between ensemble modelling (dotted and filled lines) and experiment (solid lines). Bulk ensemble absorption (blue), fluorescence (red), and fluorescence excitation anisotropy (dark green) spectra of LH2 complexes from *Rps. acidophila* measured at 4.5 K are compared to the sum of the excitation (black) and the summed fluorescence (dark red) spectra of 26 individual complexes recorded at 1.2 K. The two minima of the florescence anisotropy spectrum, indicated by arrows, are associated with the edges of the B850 exciton state manifold. The spectra in the lower panel are normalized with respect to the B850 absorption/fluorescence peak intensity.

We fitted the model to the experimental ensemble data and then steered the fitting to keep the measured Huang-Rhys factors within the region predicted by the model, maintaining the ensemble fit at the same time. The modelled ensemble spectra can be seen next to experimental ensemble spectra in Fig. 10.4. It can be seen that the model is capable of reproducing the excitation, fluorescence and fluorescence excitation anisotropy spectra on a satisfactory level. This shows that the model is applicable on the ensemble scale. The small discrepancies might come from the fact that the ensemble spectra were likely not from the exactly same sample and were definitely collected at different times, and therefore the modelling might not work as well as it should [146,147].

To study the applicability of the model on the single-complex scale, we attempted to reproduce the same distribution of individual single-complex spectra. The results of this analysis can be seen in Fig. 10.5 (a), where we superimpose the distribution of measured complexes and complexes predicted by the theoretical model. To be also able to verify the intra-complex disorder, we provide the medians and first and third quartiles of the distributions of respective parameters. It can be seen that the measured spectra overlap with the theoretically predicted spectra, but the theoretically predicted spectrum is wider, as expected.

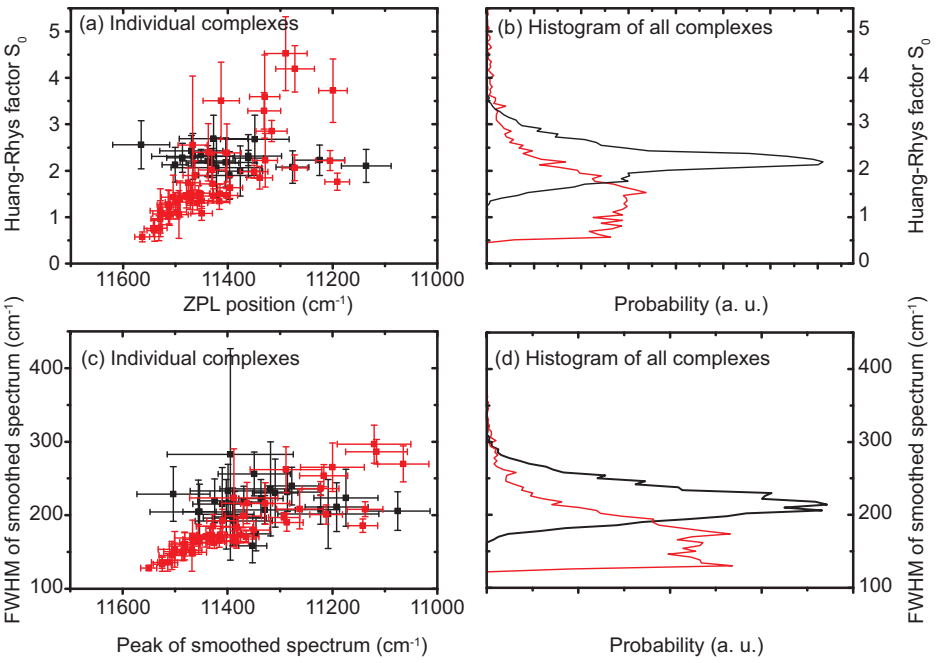

Figure 10.5. (a) Modelled $k = 0$ state Huang-Rhys factors S_0 and ZPL positions for 50 single complexes (50 realizations of inter-complex disorder corresponding to 50 complexes and 500 realizations of internal disorder per complex) as red and fitted factors from fitting of single-complex spectra as black box plots (same 17 complexes as in Fig. 10.3). The symbol in the middle shows the position of the median of the ZPL and Huang-Rhys factor distributions and the error bars show the first and third quartiles of the respective distributions for each complex. (b) The histogram of all fitted S_0 Huang-Rhys factors (black) and the histogram of the model (red, calculated for an ensemble of 5000 realizations of both inter- and intra-complex disorder). It can be seen that the experimental spectra are exclusively from the polaronic tail of the histogram. (b) and (c) represent the same analysis for the peak positions and FWHMs of individual smoothed spectra from single complexes. In this case, all of the 26 measured complexes could be taken into account and plotted.

In figure 10.5 (b) we provide the histogram of the determined Huang-Rhys factors, sampled from 5000 realizations of both inter- and intra-complex disorder. When this is compared to the histogram of Huang-Rhys factors obtained from the experiment, it is evident that the single-complex experiment is heavily biased towards the higher Huang-Rhys factor complexes, which we called polaron-like in this work due their more pronounced characteristics, such as high red-shifts and splitting of the B850 band.

To verify that the bias is not caused by the Huang-Rhys factor fitting step, we also smoothed all of the individual single-complex spectra with a Gaussian with the FWHM of 110 cm^{-1} and then determined the peak positions and FWHMs of the resulting smooth spectra. The results of this analysis, alongside

modelling results for the same approach, can be found in the Fig. 10.5 (c) and (d). The processing and plotting of this data was done as in Fig. 10.5 (a) and (b), although, since fitting was not needed, all of the measured single complexes could be used. It can be seen that the behaviour is identical to that of the Huang-Rhys factors and therefore we can conclude that the fitting step does not introduce additional biases.

Figure 10.5 also shows that there is a clear dependency between the Huang-Rhys factors and ZPL positions from any complex. Qualitatively the more self-trapped states are more red-shifted and have higher Huang-Rhys factors. This likely comes from the fact that the STE traps into the lowest possible energy configuration, which is a set of low-energy states within the B850 ring. The lower the energy of those states is, the more the exciton self-traps into that region, causing a lower delocalization length and a higher participation ratio, which leads to a higher Huang-Rhys factor.

While the behaviour seen in the LH2 complex seems very similar to what was reported in Paper I for simpler pigments, the mechanisms behind these are likely different, since in the case of the LH2 complex the excitonic interaction and self-trapping are the culprits. In the case of the simpler pigments, the exact reason for the dependency between the ZPLs and Huang-Rhys factors remains to be discovered. The same mechanism should eventually be introduced into the current excitonic mode

A set of modelled single molecules spectra can be found in Fig. 10.6. There, four calculated examples of summed spectra, analogous to Fig. 10.1 are shown. It can be seen that the spectral characteristics of complexes vary greatly. It can also be seen that complexes that exhibit higher Huang-Rhys factors have generally more red-shifted emission spectra and generally more split B850 band. Therefore it is also evident why the sum of the excitation and fluorescence spectra of all measured complexes behaves as it does compared to the ensemble spectra. When the measurement is biased toward more self-trapped states, the resulting summed B850 band would be wider and the fluorescence more red-shifted. It can also be seen that more trapped complexes exhibit wider exciton zone, which has been predicted earlier also [148].

All in all, these effects also explain the differences between the ensemble spectra and single-complex spectra in Fig. 10.4. Our conclusion is that only very polaronic complexes were included in single-complex measurements. These complexes exhibit both more red-shifted emission spectra and more split fluorescence spectra, therefore the sum of the spectra from these complexes would be wider for absorption and more red-shifted for emission.

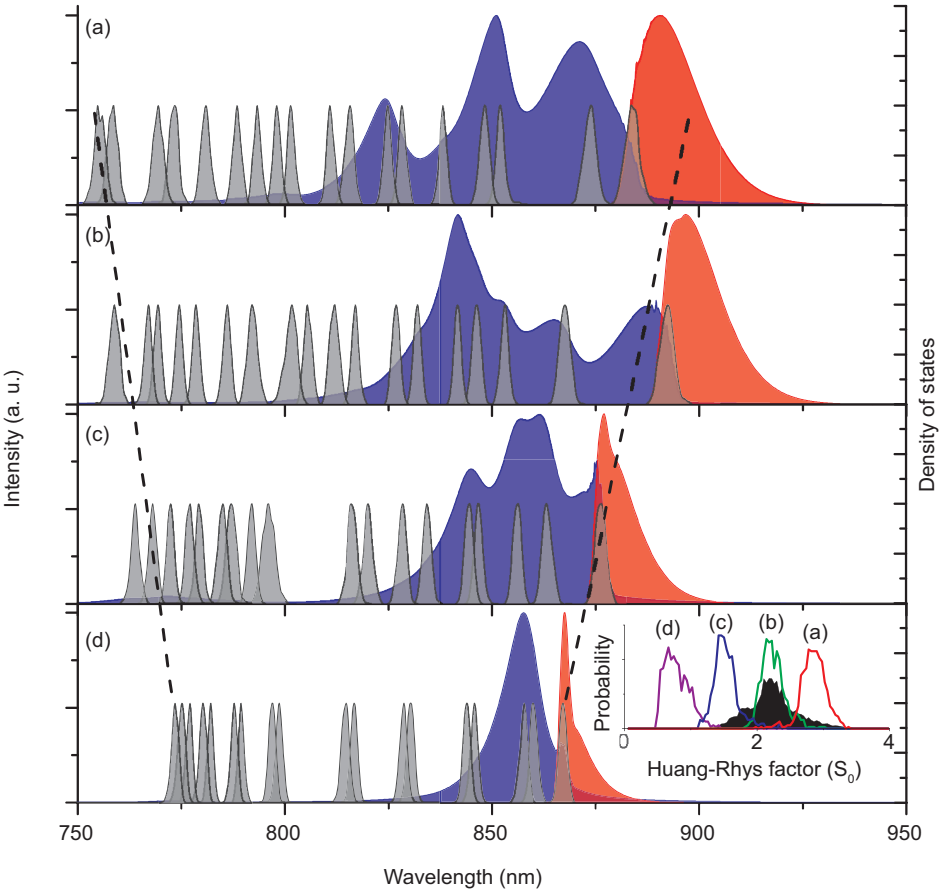

Figure 10.6. Examples of modelled single-complex spectra, integrated over time (comparable to Fig. 10.1). Absorption spectra are shown as blue filled lines, emission spectra as red filled lines. Different panels contain spectra from different complexes, the distribution of S_0 Huang-Rhys factors (histogram) is shown for each complex in lower right. From lower to upper the spectra become more polaronic, (d) being the most excitonic and the (a) the most polaronic.

The reasons for this selection could come from the fact that the more red-shifted spectra are easier to measure, since it is easier to block out the exciting laser light.

In Fig. 10.7 (a) we show that the relative intensities of emission are smaller for the less self-trapped states, leading to a good explanation to the experimental bias: the complexes measured were just significantly brighter and therefore easier to measure in the single-complex experiment.

In Fig. 10.7 (b) we also present the distribution of ZPL energies in an ensemble. It is clearly visible that the measured complexes are on the low-energy side of this distribution. The same histogram holds also deeper importance to the modelling of the LH2 complex: it is at the same time the

distribution of $k = 0$ states and the inhomogeneous distribution function used in the fluorescence line-narrowing studies. The distribution is far from being a Gaussian, as a long tail of states extends to the low-energy tail.

This data also is significant for the conventional theory of fluorescence line narrowing: in the current approach of modelling, the ΔFLN and FLN spectra cannot be used in case of excitonic interaction and disorder, as the Huang-Rhys factors change greatly and the IDF is far from Gaussian, leading to the update in the ΔFLN and FLN equations, as described in the theory section.

To show the general dependencies between the widths of spectra and to exemplify the experimental bias once more, in the most clear and robust way, we provide the peak positions and FWHMs for a set of 50 calculated summed fluorescence spectra and the summed spectra of the 26 measured complexes, all smoothed with a Gaussian with the FWHM of 110 cm^{-1}, alongside each other. The results in Fig. 10.8 show that the model produces a clear dependency between the widths of spectra and their peak positions and that the narrower and less red-shifted complexes are clearly absent from the present experimental dataset.

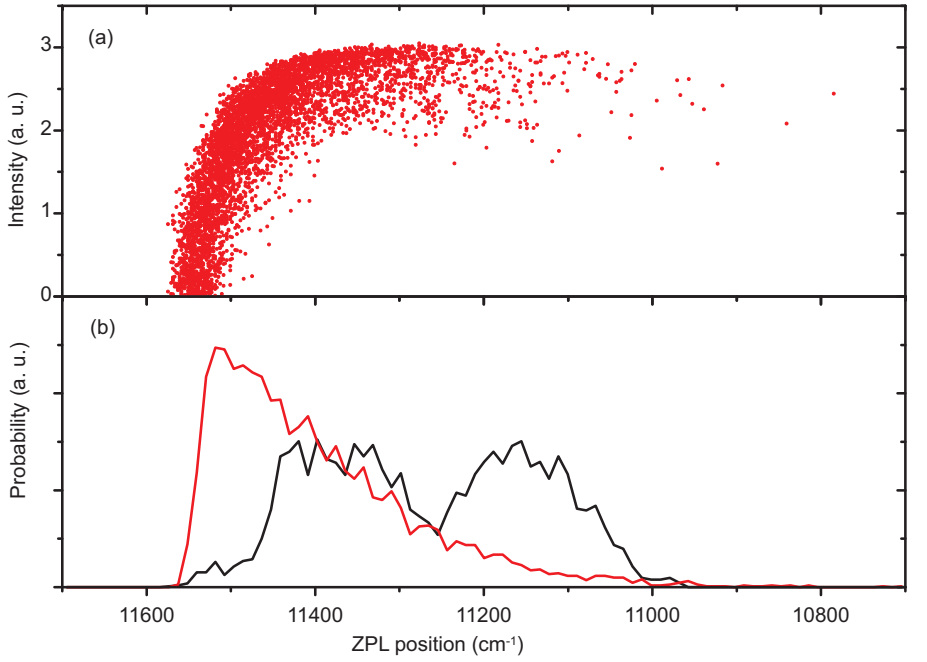

Figure 10.7. (a) Dependence between the relative intensity of emission spectra (squares of dipole moments) versus ZPL positions. Calculated from 5000 realizations of both intra- and inter-complex disorders (one intra-complex disorder per inter-complex disorder). (b) Histogram of ZPL positions for the same modeled data (i.e. the $k = 0$ energy distribution, or the IDF in the fluorescence line narrowing terminology) (red) and from the experiment (black).

As an added detail, this model confirmed that the site Huang-Rhys factor has to be very high, around 8.8, as already discussed in the previous chapter. Also, we managed to determine that the major source of inter-complex disorder is the elliptic disorder, which is relatively static in time. The intra-complex disorder is minor, but essential to model the variances within the spectra from a single complex (as in Fig. 10.3).

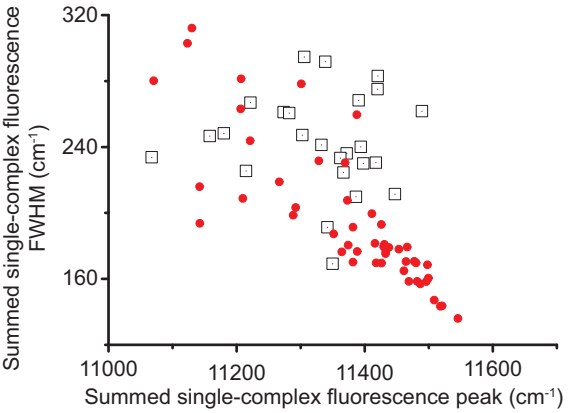

Figure 10.8. Dependence between the peaks and widths of the smoothed sums of single-complex emission spectra. The experimentally measured 26 complexes are shown as squares and the modeled 50 complexes as red circles.

SUMMARY AND THE MAIN RESULTS

We set out to better understand the excitonic interactions in photosynthetic light-harvesting complexes and to test the resilience of the photosynthetic excitons against rising temperatures and increasing levels of organizational complexity.

Toward this end, we performed measurements on LH2, one of the role models of photosynthetic antenna exciton systems, as well as on other bacterial LH complexes. Some simpler molecules that are important to photosynthesis were also studied. To analyse the spectral behaviour seen in the experiments, we constructed a disordered self-trapped exciton model to predict the characteristics and thermal evolution of excitons. As a result, we were able to interpret a wide set of experimental results from fluorescence, absorption, and fluorescence excitation anisotropy studies. Most importantly, we managed to prove that excitons remain valid for isolated LH2 complexes at room temperature and that their characteristics change only a little compared to the low-temperature limit.

We then moved on to measurements of light-harvesting samples of increasing complexity, from isolated complexes to full photosynthetic membranes, and even to complete bacterial cells at room temperature. While the signatures of excitons are weak at biological conditions (mostly due to depolarization due to other components of the cell and widening of spectral lineshapes), they are definitely present.

To characterize these biologically relevant excitons in more detail, we thoroughly studied their spectra at low temperatures, first in ensembles and later in single complexes. Based on single complex spectra, a very detailed model was developed, explaining all the main characteristics of photosynthetic self-trapped excitons, and especially, revealing the disorder effect on the spectral behaviour of the complexes.

The main results of this work are as follows:

- Excitons are present in the cells of photosynthetic bacteria at physiological conditions.
- Higher temperatures have only a small effect on the exciton coupling energy and the exciton band width for the antenna complexes from purple bacteria. The exciton band in different complexes (LH2 and LH1) shrinks only by 8 to 16 %, respectively, between the cryogenic and physiological temperatures.
- The disordered self-trapped exciton model adequately describes the main spectroscopic properties of excitons in LH2 complexes studied in this work, confirming that self-trapping is an essential feature of photosynthetic excitons.

- Interpretation of the single complex spectra necessarily requires distinction between the inter- and intra-complex disorders and we assembled a new theoretical model to describe that.
- The coupling to phonons greatly increases when BChls are integrated into the protein matrix of light-harvesting complexes, compared to the same pigments in localized or in weakly excitonically interacting systems.

SUMMARY IN ESTONIAN

Lokaliseerunud fotosünteetilised eksitonid

Töö põhieesmärgiks oli fotosünteetilistes kompleksides esinevat eksitoninteraktsiooni, eriti eksitonide iselõksustumist, paremini tundma õppida ja uurida kui hästi peab fotosünteetilistes valgukompleksides esinev eksitoninteraktsioon vastu, kui temperatuure ja süsteemide keerukust tõsta.

Selleks mõõtsime LH2 – ühe tuntuima fotosünteetilise antennikompleksi – ja teiste valgust koguvate antennikomplekside optilisi spektreid. Samuti uurisime lihtsamaid fotosünteesiks vajalikke molekule. Eksperimendis nähtu seletamiseks lõime matemaatilise mudeli, mis ennustab komplekside omadusi ja termilist käitumist lähtuvalt iselõksustuvate eksitonide mudelist (kasutasime nii Holsteini kui ka Su-Schrieffer-Heegeri hamiltoniaane). See mudel võimaldas tõlgendada suurest hulgast fluorestsentsi, neelduvuse ja fluorestsentsi anisotroopia katsetest pärinevaid andmeid ja tõestada, et eksitonmudel jääb LH2 kompleksides kehtima ka toatemperatuuril ja et komplekside eksitonomadused erinevad küllalki vähe absoluutse nulli lähedaste temperatuuride juures mõõdetuist.

Seejärel liikusime edasi erinevate valgust koguvate komplekside uurimise juurde, tõstes süsteemi keerukust isoleeritud kompleksidest membraanideni, mis sisaldasid mitut tüüpi komplekse, ja lõpuks jõudsime täielike bakterirakkudeni toatemperatuuril. Kuigi eksitonide tundemärgid on bioloogilistes tingimustes nõrgad (tõenäoliselt põhiliselt muude rakus olevate komponentide depolariseeriva mõju tõttu), jääb eksitoninteraktsiooni tugevus ligilähedaseks absoluutse nulli lähedal eraldatud kompleksides mõõdetuga.

Nende, nüüd ka tõestatult bioloogilist tähendust omavate eksitonide täpsemaks iseloomustamiseks uurisime nende spektreid madalatel temperatuuridel, esialgu suurtes ansamblites ja hiljem ühekaupa. Ühe kompleksi spektroskoopiale tuginedes lõime väga detailse mudeli, mis seletab kõiki iselõksustunud eksitonide põhilisi omadusi ja eriti nende sisemise korrastamatuse mõju spektraalsele käitumisele.

Selle töö põhitulemused on:

- Eksitonid eksisteerivad fotosünteesivate bakterite rakkudes füsioloogilistel temperatuuridel.
- Temperatuuri tõstmine mõjutab eksitoninteraktsiooni tugevust ja eksitontsooni laiust vähe. Eksitonriba laius väheneb temperatuuri tõustes väga madalatelt krüogeenilistelt temperatuuridelt toatemperatuurini erinevates kompleksides (LH2 ja LH1) ainult vastavalt 8–16%.
- Korrastamatuse ja iselõksustumisega eksitonmudel kirjeldab LH2 kompleksides esinevate eksitonide spektroskoopilisi omadusi piisavalt hästi, näidates, et iselõksustumine on fotosünteetiliste eksitonide oluline omadus.

- Me leidsime, et ühe kompleksi spektrite interpreteerimiseks on vaja eristada kompleksisisest ja kompleksivälist korrastamatust ning panime selleks kokku uudse mudeli.
- Foononinteraktsiooni tugevus suureneb oluliselt, kui fotosünteetilised pigmendid paigutada valgust koguvate antennikomplekside koosseisu võrreldes samade pigmentidega nõrga vastastikmõjuga süsteemides.

ACKNOWLEDGEMENTS

Firstly, I would like to thank my supervisors, Professor Arvi Freiberg and Dr. Margus Rätsep, for patiently supervising me from the start of my bachelor's studies to the end of my Ph. D. studies. Dr. Margus Rätsep taught me all of the skills required for performing the experiments and analysing experimental data, and Professor Arvi Freiberg helped with the theory. I would also like to thank both of Prof. Arvi Freiberg and Dr. Margus Rätsep for writing and/or co-writing the papers this thesis is based on and for helping me with my contributions, and of course the Ph. D. thesis itself. I would also like to thank Dr. Gediminas Trinkunas from the Center for Physical Sciences and Technology in Vilnius, Lithuania for teaching me the basics of modelling spectra based on the excitonic model, sharing his programs and helping me with theoretical aspects later, being also a co-author for Paper II.

I would also like to thank other members of the laboratory of biophysics: Dr. Liina Kangur, who helped me with high-pressure cell and sample preparation for experiments; Hain Salujärv and Agu Anijalg, who helped to construct parts of the experimental apparatus; Dr. Kristjan Leiger, who helped with an older version of the pressure cell; Dr. Juha Matti Linnanto, who performed the modelling in Paper V; Dr. Kõu Timpmann, who helped with samples and provided input for the final paper; and Dr. Erko Jalviste.

Thanks go out also for Prof. Jürgen Köhler and Dr. Ralf Kunz from Bayreuth Institute for Macromolecular Research, University of Bayreuth, Germany, for providing the single-complex data we used in our Paper VI (Dr. Kõu Timpmann also took part in these measurements). Also, we would like to thank Prof. C. Neil Hunter for providing the samples we have measured and Prof. Tõnu Pullerits for sharing his programs and providing articles for simulating the temperature dependence of spectral lineshapes.

This work has been partially supported by graduate school "Functional materials and technologies," receiving funding from the European Social Fund under project 1.2.0401.09-0079 in Estonia, by European Social Fund's Doctoral Studies and Internationalisation Programme DoRa, and the Kristjan Jaak scholarships from the Archimedes foundation.

REFERENCES

1. Longuet-Higgins, H. C. Quantum mechanics and biology. *Biophys. J.*, 1962, **2**, 207–215.
2. Arndt, M., Juffmann, T., and Vedral, V. Quantum physics meets biology. *HFSP J.*, 2009, **3**, 386–400.
3. Abbot, D., Davies, P. C., and Pati, A. K. *Quantum aspects of life*, Imperial College Press, London, 2008.
4. Sánchez-Mosteiro, G., Koopman, M., van Dijk, E. M. H. P., Hernando, J., van Hulst, N. F., and García-Parajó, M. F. Photon antibunching proves emission from a single subunit in the autofluorescent protein dsred. *ChemPhysChem*, 2004, **5**, 1782–1785.
5. Hackermüller, L., Uttenthaler, S., Hornberger, K., Reiger, E., Brezger, B., Zeilinger, A., et al. Wave nature of biomolecules and fluorofullerenes. *Phys. Rev. Lett.*, 2003, **91**, 090408.
6. Jones, J. A. and Mosca, M. Approximate quantum counting on an nmr ensemble quantum computer. *Phys. Rev. Lett.*, 1999, **83**, 1050–1053.
7. Cha, Y., Murray, C., and Klinman, J. Hydrogen tunneling in enzyme reactions. *Science*, 1989, **243**, 1325–1330.
8. Glickman, M. H., Wiseman, J. S., and Klinman, J. P. Extremely large isotope effects in the soybean lipoxygenase-linoleic acid reaction. *J. Am. Chem. Soc.*, 1994, **116**, 793–794.
9. Van Amerongen, H., Valkunas, L., and Van Grondelle, R. *Photosynthetic excitons*, World Scientific, Singapore, 2000.
10. Markvart, T. Light harvesting for quantum solar conversion. *Prog. Quant. Electr.*, 2000, **24**, 107–186.
11. Laisk, A., Nedbal, L., and Govindjee, (Eds.) (2009) *Photosynthesis in silico. Understanding complexity from molecules to ecosystems*, Springer, Heidelberg.
12. McKemmish, L. K., McKenzie, R. H., Hush, N. S., and Reimers, J. R. Quantum entangelment between electronic and vibrational degrees of freedom in molecules. *J. Chem. Phys.*, 2011, **135**, 244110.
13. Frenkel, J. On the transformation on light into heat in solids. Ii. *Phys. Rev.*, 1931, **37**, 1276–1294.
14. Cogdell, R. J., Gall, A., and Köhler, J. The architecture and function of the light-harvesting apparatus of purple bacteria: From single molecules to in vivo membranes. *Quart. Rev. Biophys.*, 2006, **39**, 227–324.
15. Scholes, G. D. and Rumbles, G. Excitons in nanoscale systems. *Nature Materials*, 2006, **5**, 683–693.
16. Freiberg, A. and Trinkunas, G. (2009) Unraveling the hidden nature of antenna excitations, In *Photosynthesis in silico. Understanding complexity from molecules to ecosystems* (Laisk, A., Nedbal, L., Govindjee, Ed.), pp 55–82, Springer, Heidelberg.

17. Eisele, D. M., Arias, D. H., Fu, X., Bloemsma, E. A., Steiner, C. P., Jensen, R. A., et al. Robust excitons inhabit soft supramolecular nanotubes. *Proc. Natl. Acad. Sci. USA*, 2014, **111**, E3367–E3375.
18. Panitchayangkoon, G., Hayes, D., Fransted, K. A., Caram, J. R., Harel, E., Wen, J., et al. Long-lived quantum coherence in photosynthetic complexes at physiological temperature. *Proc. Natl. Acad. Sci. USA*, 2010, **107**, 12766–12770.
19. Harel, E. and Engel, G. S. Quantum coherence spectroscopy reveals complex dynamics in bacterial light-harvesting complex 2 (lh2). *Proc. Natl. Acad. Sci. USA*, 2012, **109**, 707–711.
20. Panitchayangkoon, G., Voronine, D. V., Abramavicius, D., Caram, J. R., Lewis, N. H. C., Mukamel, S., et al. Direct evidence of quantum transport in photosynthetic light-harvesting complexes. *Proc. Natl. Acad. Sci. USA*, 2011, **108**, 20909–20912.
21. Wolynes, P. G. Some quantum weirdness in physiology. *Proc. Natl. Acad. Sci. USA*, 2009, **106**, 17247–17248.
22. Davydov, A. S. *Theory of molecular excitons*, Plenum Press, New York, 1971.
23. Toyozawa, Y. *Optical processes in solids*, Cambridge University Press, Cambridge, 2003.
24. Harris, C. B. and Zwemer, D. A. Coherent energy transfer in solids. *Ann. Rev. Phys. Chem.*, 1978, **29**, 473–495.
25. Freiberg, A., Pajusalu, M., and Rätsep, M. Excitons in intact cells of photosynthetic bacteria. *J. Phys. Chem. B*, 2013, **117**, 11007–11014.
26. Şener, M., Strümpfer, J., Timney, J. A., Freiberg, A., Hunter, C. N., and Schulten, K. Photosynthetic vesicle architecture and constraints on efficient energy transfer. *Biophys. J.*, 2010, **99**, 67–75.
27. Şener, M., Hsin, J., Trabuco, L. G., Villa, E., Qian, P., Hunter, C. N., et al. Structural model and excitonic properties of the dimeric rc-lh1-pufx complex from rhodobacter sphaeroides. *Chem. Phys.*, 2009, **357**, 188–197.
28. Cherezov, V., Clogston, J., Papiz, M. Z., and Caffrey, M. Room to move: Crystallizing membrane proteins in swollen lipidic mesophases. *J. Mol. Biol.*, 2006, **357**, 1605–1618.
29. Xu, D. and Zhang, Y. Generating triangulated macromolecular surfaces by euclidean distance transform. *PLoS ONE*, 2009, **4**, e8140.
30. Blankenship, R. E., Madigan, M. T., and Bauer, C. E., (Eds.) (1995) *Anoxygenic photosynthetic bacteria*, Kluwer Academic Publishers, Dordrecht.
31. Bullough, P. A., Qian, P., and Hunter, C. N. (2009) Reaction center-light-harvesting core complexes of purple bacteria, In *The purple phototrophic bacteria* (Hunter, C. N., Daldal, F., Thurnauer, M.C., Beatty, J.T., Ed.), Springer, Dordrecht, the Netherlands.

32. Jungas, C., Ranck, J. L., Rigaud, J. L., Joliot, P., and Vermeglio, A. Supramolecular organization of the photosynthetic apparatus of *rhodobacter sphaeroides*. *EMBO J.*, 1999, **18**, 534–542.
33. Walz, T., Jamieson, S. J., Bowers, C. M., Bullough, P. A., and Hunter, C. N. Projection structures of three photosynthetic complexes from *rhodobacter sphaeroides*: Lh2 at 6 a, lh1 and rc-lh1 at 25 a. *J. Mol. Biol.*, 1998, **282**, 833–845.
34. Freiberg, A. (1995) Coupling of antennas to reaction centers, In *Anoxygenic photosynthetic bacteria* (Blankenship, R. E., Madigan, M. T., and Bauer, C. E., Eds.), pp 385–398, Kluwer Academic Publishers, Dordrecht, The Netherlands.
35. Vredenberg, W. J. and Duysens, L. N. M. Transfer of energy from bacteriochlorophyll to a reaction centre during bacterial photosynthesis. *Nature*, 1963, **197**, 355–357.
36. Papiz, M. Z., Prince, S. M., Howard, T., Cogdell, R. J., and Isaacs, N. W. The structure and thermal motion of the b800-850 lh2 complex from *rps. Acidophila* at 2.0 a resolution at 100 k: New structural features and functionally relevant motions. *J. Mol. Biol.*, 2003, **326**, 1523–1538.
37. McDermott, G., Prince, S. M., Freer, A. A., Hawthornthwaite-Lawless, A. M., Papiz, M. Z., Cogdell, R. J., et al. Crystal structure of an integral membrane light-harvesting complex from photosynthetic bacteria. *Nature*, 1995, **374**, 517–521.
38. Sundström, V., Pullerits, T., and van Grondelle, R. Photosynthetic light-harvesting: Reconciling dynamics and structure of purple bacterial lh2 reveals function of photosynthetic unit. *J. Phys. Chem. B*, 1999, **103**, 2327–2346.
39. Sumi, H. Bacterial photosynthesis begins with quantum-mechanical coherence. *Chem. Rec.*, 2001, **1**, 480–493.
40. Hu, X., Ritz, T., Damjanovic, A., Autenrieth, F., and Schulten, K. Photosynthetic apparatus of purple bacteria. *Quart. Rev. Biophys.*, 2002, **35**, 1–62.
41. Novoderezhkin, V. I. and van Grondelle, R. Physical origins and models of energy transfer in photosynthetic light-harvesting. *Phys. Chem. Chem. Phys.*, 2010, **12**, 7352–7365.
42. Timpmann, K., Katiliene, Z., Woodbury, N. W., and Freiberg, A. Exciton self-trapping in one-dimensional photosynthetic antennas. *J. Phys. Chem. B*, 2001, **105**, 12223–12225.
43. Damjanovic, A., Kosztin, I., Kleinekathöfer, U., and Schulten, K. Excitons in a photosynthetic light-harvesting system: A combined molecular dynamics, quantum chemistry, and polaron model study. *Phys. Rev. E*, 2002, **65**, 031919–031943.
44. Freiberg, A., Rätsep, M., Timpmann, K., and Trinkunas, G. Excitonic polarons in quasi-one-dimensional lh1 and lh2 bacteriochlorophyll a

antenna aggregates from photosynthetic bacteria: A wavelength-dependent selective spectroscopy study. *Chem. Phys.*, 2009, **357**, 102–112.
45. Freiberg, A., Rätsep, M., Timpmann, K., and Trinkunas, G. Self-trapped excitons in circular bacteriochlorophyll antenna complexes. *J. Lumin.*, 2003, **102–103**, 363–368.
46. Freiberg, A., Rätsep, M., Timpmann, K., Trinkunas, G., and Woodbury, N. W. Self-trapped excitons in lh2 antenna complexes between 5 k and ambient temperature. *J. Phys. Chem. B*, 2003, **107**, 11510–11519.
47. Polivka, T., Pullerits, T., Herek, J. L., and Sundström, V. Exciton relaxation and polaron formation in lh2 at low temperature. *J. Phys. Chem. B*, 2000, **104**, 1088–1096.
48. Moreland, J., Gramada, A., Buzko, O., Zhang, Q., and Bourne, P. The molecular biology toolkit (mbt): A modular platform for developing molecular visualization applications. *BMC Bioinf.*, 2005, **6**, 21.
49. Krueger, B. P., Scholes, G. D., and Fleming, G. R. Calculation of couplings and energy-transfer pathways between the pigments of lh2 by the ab initio transition density cube method. *J. Phys. Chem. B*, 1998, **102**, 5378–5386.
50. Freer, A., Prince, S., Sauer, K., Papiz, M., Lawless, A. H., McDermott, G., et al. Pigment–pigment interactions and energy transfer in the antenna complex of the photosynthetic bacterium rhodopseudomonas acidophila. *Structure*, 1996, **4**, 449–462.
51. Jang, S., Dempster, S. E., and Silbey, R. J. Characterization of the static disorder in the b850 band of lh2†. *J. Phys. Chem. B*, 2001, **105**, 6655–6665.
52. Neugebauer, J. Photophysical properties of natural light-harvesting complexes studied by subsystem density functional theory. *J. Phys. Chem. B*, 2008, **112**, 2207–2217.
53. Scholes, G. D., Gould, I. R., Cogdell, R. J., and Fleming, G. R. Ab initio molecular orbital calculations of electronic couplings in the lh2 bacterial light-harvesting complex of rps. Acidophila. *J. Phys. Chem. B*, 1999, **103**, 2543–2553.
54. Hofmann, C., Aartsma, T. J., and Köhler, J. Energetic disorder and the b850-exciton states of individual light-harvesting 2 complexes from rhodopseudomonas acidophila. *Chem. Phys. Lett.*, 2004, **395**, 373–378.
55. Gall, A., Sogaila, E., Gulbinas, V., Ilioaia, O., Robert, B., and Valkunas, L. Spectral dependence of energy transfer in wild-type peripheral light-harvesting complexes of photosynthetic bacteria. *Biochim. Biophys. Acta Bioenergetics*, 2010, **1797**, 1465–1469.
56. Wu, H. M., Savikhin, S., Reddy, N. R. S., Jankowiak, R., Cogdell, R. J., Struve, W. S., et al. Femtosecond and hole-burning studies of b800's excitation energy relaxation dynamics in the lh2 antenna complex of rhodopseudomonas acidophila (strain 10050). *J. Phys. Chem.*, 1996, **100**, 12022–12033.

57. Liuolia, V., Valkunas, L., and van Grondelle, R. Excitons in dimerized chains. *J. Phys. Chem. B*, 1997, **101**, 7343–7349.
58. Koolhaas, M. H. C., Frese, R. N., Fowler, G. J. S., Bibby, T. S., Georgakopoulou, S., van der Zwan, G., et al. Identification of the upper exciton component of the b850 bacteriochlorophylls of the lh2 antenna complex, using a b800-free mutant of rhodobacter sphaeroides†. *Biochem.*, 1998, **37**, 4693–4698.
59. Scholes, G. D. and Fleming, G. R. On the mechanism of light harvesting in photosynthetic purple bacteria: B800 to b850 energy transfer. *J. Phys. Chem. B*, 2000, **104**, 1854–1868.
60. Jang, S., Silbey, R. J., Kunz, R., Hofmann, C., and Köhler, J. Is there elliptic distortion in the light harvesting complex 2 of purple bacteria? *J. Phys. Chem. B*, 2011, **115**, 12947–12953.
61. Tubasum, S., Camacho, R., Meyer, M., Yadav, D., Cogdell, R. J., Pullerits, T., et al. Evidence of excited state localization and static disorder in lh2 investigated by 2d-polarization single-molecule imaging at room temperature. *Phys. Chem. Chem. Phys.*, 2013, **15**, 19862–19869.
62. Ketelaars, M., van Oijen, A. M., Matsushita, M., Köhler, J., Schmidt, J., and Aartsma, T. J. Spectroscopy on the b850 band of individual light-harvesting 2 complexes of rhodopseudomonas acidophila i. Experiments and monte carlo simulations. *Biophys. J.*, 2001, **80**, 1591–1603.
63. Hong, X., Weng, Y.-X., and Li, M. Determination of the topological shape of integral membrane protein light-harvesting complex lh2 from photosynthetic bacteria in the detergent solution by small-angle x-ray scattering. *Biophys. J.*, 2004, **86**, 1082–1088.
64. Pajusalu, M., Rätsep, M., Trinkunas, G., and Freiberg, A. Davydov splitting of excitons in cyclic bacteriochlorophyll a nanoaggregates of bacterial light-harvesting complexes between 4.5 and 263 k. *ChemPhysChem*, 2011, **12**, 634–644.
65. Timpmann, K., Trinkunas, G., Olsen, J. D., Neil Hunter, C., and Freiberg, A. Bandwidth of excitons in lh2 bacterial antenna chromoproteins. *Chem. Phys. Lett.*, 2004, **398**, 384–388.
66. Freiberg, A., Rätsep, M., and Timpmann, K. A comparative spectroscopic and kinetic study of photoexcitations in detergent-isolated and membrane-embedded lh2 light-harvesting complexes. *Biochim. Biophys. Acta Bioenergetics*, 2012, **1817**, 1471–1482.
67. Georgakopoulou, S., Frese, R. N., Johnson, E., Koolhaas, C., Cogdell, R. J., van Grondelle, R., et al. Absorption and cd spectroscopy and modeling of various lh2 complexes from purple bacteria. *Biophys. J.*, 2002, **82**, 2184–2197.
68. Freiberg, A., Godik, V. I., Pullerits, T., and Timpmann, K. Picosecond dynamics of directed excitation transfer in spectrally heterogeneous light-harvesting antenna of purple bacteria. *Biochim. Biophys. Acta*, 1989, **973**, 93–104.

69. Reddy, N. R. S., Small, G. J., Seibert, M., and Picorel, R. Energy transfer dynamics of the b800–b850 complex of *rhodobacter sphaeroides*: A hole burning study. *Chem. Phys. Lett.*, 1991, **181**, 391–399.
70. Jimenez, R., Dikshit, S. N., Bradforth, S. E., and Fleming, G. R. Electronic excitation transfer in the lh2 complex of *rhodobacter sphaeroides*. *J. Phys. Chem.*, 1996, **100**, 6825–6834.
71. Kuhn, O. and Sundstrom, V. Pump-probe spectroscopy of dissipative energy transfer dynamics in photosynthetic antenna complexes: A density matrix approach. *Journal of Chem. Phys.*, 1997, **107**, 4154–4164.
72. Freiberg, A., Timpmann, K., Lin, S., and Woodbury, N. W. Exciton relaxation and transfer in the lh2 antenna network of photosynthetic bacteria. *J. Phys. Chem. B*, 1998, **102**, 10974–10982.
73. May, V. and Kühn, O. *Charge and energy transfer dynamics in molecular systems: A theoretical introduction*, Wiley-VCH, Berlin, 2000.
74. Book, L. D., Ostafin, A. E., Ponomarenko, N., Norris, J. R., and Scherer, N., F, Exciton delocalization and initial dephasing dynamics of purple bacterial lh2. *J. Phys. Chem. B*, 2000, **104**, 8295–8307.
75. Hsin, J., Struempfer, J., Şener, M., Qian, P., Hunter, C. N., and Schulten, K. Energy transfer dynamics in an rc-lh1-pufx tubular photosynthetic membrane. *New J. Phys.*, 2010, **12**, 19.
76. Borisov, A. Y., Freiberg, A. M., Godik, V. I., Rebane, K., and Timpmann, K. Kinetics of picosecond bacteriochlorophyll luminescence in vivo as a function of the reaction center state. *Biochim. Biophys. Acta*, 1985, **807**, 221–229.
77. van Grondelle, R., Dekker, J. P., Gillbro, T., and Sundstrom, V. Energy transfer and trapping in photosynthesis. *Biochim. Biophys. Acta Bio-energetics*, 1994, **1187**, 1–65.
78. Freiberg, A., Allen, J. P., Williams, J., and Woodbury, N. W. Energy trapping and detrapping by wild type and mutant reaction centers of purple non-sulfur bacteria. *Photosynth. Res.*, 1996, **48**, 309–319.
79. Timpmann, K., Woodbury, N. W., and Freiberg, A. Unraveling exciton relaxation and energy transfer in lh2 photosynthetic antennas. *J. Phys. Chem. B*, 2000, **104**, 9769–9771.
80. Linnanto, J., Freiberg, A., and Korppi-Tommola, J. Quantum chemical simulations of excited-state absorption spectra of photosynthetic bacterial reaction center and antenna complexes. *J. Phys. Chem. B*, 2011, **115**, 5536–5544.
81. Renger, T. and Marcus, R. A. On the relation of protein dynamics and exciton relaxation in pigment – protein complexes: An estimation of the spectral density and a theory for the calculation of optical spectra. *J. Chem. Phys.*, 2002, **116**, 9997–10019.
82. Alden, R. G., Johnson, E., Nagarajan, V., Parson, W. W., Law, C. J., and Cogdell, R. G. Calculations of spectroscopic properties of the lh2

bacteriochlorophyll−protein antenna complex from rhodopseudomonas acidophila†. *J. Phys. Chem. B*, 1997, **101**, 4667–4680.
83. Jang, S. and Silbey, R. J. Single complex line shapes of the b850 band of lh2. *J. Chem. Phys.*, 2003, **118**, 9324–9336.
84. Linnanto, J., Korppi-Tommola, J. E. I., and Helenius, V. M. Electronic states, absorption spectrum and circular dichroism spectrum of the photosynthetic bacterial lh2 antenna of rhodopseudomonas acidophila as predicted by exciton theory and semiempirical calculations. *J. Phys. Chem. B*, 1999, **103**, 8739–8750.
85. Bopp, M. A., Jia, Y., Li, L., Cogdell, R. J., and Hochstrasser, R. M. Fluorescence and photobleaching dynamics of single light-harvesting complexes. *Proc. Natl. Acad. Sci. USA*, 1997, **94**, 10630–10635.
86. Matsushita, M., Ketelaars, M., van Oijen, A. M., Köhler, J., Aartsma, T. J., and Schmidt, J. Spectroscopy on the b850 band of individual light-harvesting 2 complexes of rhodopseudomonas acidophila ii. Exciton states of an elliptically deformed ring aggregate. *Biophys. J.*, 2001, **80**, 1604–1614.
87. van Oijen, A. M., Ketelaars, M., Köhler, J., Aartsma, T. J., and Schmidt, J. Spectroscopy of single light-harvesting complexes from purple photosynthetic bacteria at 1.2 k. *J. Phys. Chem. B*, 1998, **102**, 9363–9366.
88. Kunz, R., Timpmann, K., Southall, J., Cogdell, R. J., Freiberg, A., and Köhler, J. Exciton self trapping in photosynthetic pigment–protein complexes studied by single-molecule spectroscopy. *J. Phys. Chem. B*, 2012, **116**, 11017–11023.
89. Kunz, R., Timpmann, K., Southall, J., Cogdell, R. J., Freiberg, A., and Köhler, J. Fluctuations in the electron–phonon coupling of a single chromoprotein. *Angew. Chem. Int. Ed. Engl.*, 2013, **52**, 8726–8730.
90. Kunz, R., Timpmann, K., Southall, J., Cogdell, R. J., Freiberg, A., and Köhler, J. Single-molecule spectroscopy unmasks the lowest exciton state of the b850 assembly in lh2 from rps. Acidophila. *Biophys. J.*, 2014, **106**, 1–9.
91. Kunz, R., Timpmann, K., Southall, J., Cogdell, R. J., Köhler, J., and Freiberg, A. Fluorescence-excitation and emission spectra from lh2 antenna complexes of rhodopseudomonas acidophila as a function of the sample preparation conditions. *J. Phys. Chem. B*, 2013, **117**, 12020–12029.
92. Tietz, C., Chekhlov, O., Dräbenstedt, A., Schuster, J., and Wrachtrup, J. Spectroscopy on single light-harvesting complexes at low temperature. *J. Phys. Chem. B*, 1999, **103**, 6328–6333.
93. Brecht, M. Spectroscopic characterization of photosystem i at the single-molecule level. *Mol. Phys.*, 2009, **107**, 1955–1974.
94. Brecht, M., Skandary, S., Hellmich, J., Glöckner, C., Konrad, A., Hussels, M., et al. Spectroscopic properties of photosystem ii core complexes from thermosynechococcus elongatus revealed by single-molecule experiments. *Biochim. Biophys. Acta Bioenergetics*, 2014, **1837**, 773–781.

95. Leiger, K., Reisberg, L., and Freiberg, A. Fluorescence micro-spectroscopy study of individual photosynthetic membrane vesicles and light-harvesting complexes. *J. Phys. Chem. B*, 2013, **117**, 9315–9326.
96. Rutkauskas, D., Novoderezkhin, V., Cogdell, R. J., and van Grondelle, R. Fluorescence spectral fluctuations of single lh2 complexes from rhodopseudomonas acidophila strain 10050. *Biochem.*, 2004, **43**, 4431–4438.
97. van Oijen, A. M., Ketelaars, M., Köhler, J., Aartsma, T. J., and Schmidt, J. Unraveling the electronic structure of individual photosynthetic pigment-protein complexes. *Science*, 1999, **285**, 400–402.
98. Cogdell, R. J. and Köhler, J. Use of single-molecule spectroscopy to tackle fundamental problems in biochemistry: Using studies on purple bacterial antenna complexes as an example. *Biochemical Journal*, 2009, **422**, 193–205.
99. Jankowiak, R., Reppert, M., Zazubovich, V., Pieper, J., and Reinot, T. Site selective and single complex laser-based spectroscopies: A window on excited state electronic structure, excitation energy transfer, and electron–phonon coupling of selected photosynthetic complexes. *Chem. Rev.*, 2011, **111**, 4546–4598.
100. Rätsep, M. and Freiberg, A. Resonant emission from the b870 exciton state and electron-phonon coupling in the lh2 antenna chromoprotein. *Chem. Phys. Lett.*, 2003, **377**, 371–376.
101. Rätsep, M. and Freiberg, A. Electron-phonon and vibronic couplings in the fmo bacteriochlorophyll a antenna complex studied by difference fluorescence line narrowing. *J. Lumin.*, 2007, **127**, 251–259.
102. Wolf, J., Law, K.-Y., and Myers, A. B. Hole-burning subtracted fluorescence line-narrowing spectroscopy of squaraines in polymer matrices. *J. Phys. Chem.*, 1996, **100**, 11870–11882.
103. Lax, M. The franck-condon principle and its application to crystals. *J. Chem. Phys.*, 1952, **20**, 1752–1760.
104. Rätsep, M., Pajusalu, M., and Freiberg, A. Wavelength-dependent electron-phonon coupling in impurity glasses. *Chem. Phys. Lett.*, 2009, **479**, 140–143.
105. Timpmann, K., Trinkunas, G., Qian, P., Hunter, C. N., and Freiberg, A. Excitons in core lh1 antenna complexes of photosynthetic bacteria: Evidence for strong resonant coupling and off-diagonal disorder. *Chem. Phys. Lett.*, 2005, **414**, 359–363.
106. Richter, M. F., Baier, J., Cogdell, R. J., Köhler, J., and Oellerich, S. Single-molecule spectroscopic characterization of light-harvesting 2 complexes reconstituted into model membranes. *Biophys. J.*, 2007, **93**, 183–191.
107. Böhm, P. S., Kunz, R., Southall, J., Cogdell, R. J., and Köhler, J. Does the reconstitution of rc-lh1 complexes from rhodopseudomonas acidophila strain 10050 into a phospholipid bilayer yield the optimum environment for optical spectroscopy? *J. Phys. Chem. B*, 2013, **117**, 15004–15013.

108. Timpmann, K., Rätsep, M., Hunter, C. N., and Freiberg, A. Emitting excitonic polaron states in core lh1 and peripheral lh2 bacterial light-harvesting complexes. *J. Phys. Chem. B*, 2004, **108**, 10581–10588.
109. Holstein, T. Studies of polaron motion. Part i. The molecular-crystal model. *Ann. Phys.*, 1959, **8**, 325–342.
110. Heeger, A. J., Kivelson, S., Schrieffer, J. R., and Su, W.-P. Solitons in conducting polymers. *Rev. Mod. Phys.*, 1988, **60**, 781–851.
111. Trinkunas, G. and Freiberg, A. A disordered polaron model for polarized fluorescence excitation spectra of lh1 and lh2 bacteriochlorophyll antenna aggregates. *J. Lumin.*, 2006, **119–120**, 105–110.
112. Noba, K. and Kayanuma, Y. Numerically rigorous results for the ground stsate of exciton-lattice systems. *J. Phys. Soc. Japan*, 1998, **67**, 3972–3975.
113. Freiberg, A., Timpmann, K., Ruus, R., and Woodbury, N. W. Disordered exciton analysis of linear and nonlinear absorption spectra of antenna bacteriochlorophyll aggregates: Lh2-only mutant chromatophores of *rhodobacter sphaeroides* at 8 k under spectrally selective excitation. *J. Phys. Chem. B*, 1999, **103**, 10032–10041.
114. van Oijen, A. M., Ketelaars, M., Köhler, J., Aartsma, T. J., and Schmidt, J. Spectroscopy of individual light-harvesting 2 complexes of rhodopseudomonas acidophila: Diagonal disorder, intercomplex heterogeneity, spectral diffusion, and energy transfer in the b800 band. *Biophys. J.*, 2000, **78**, 1570–1577.
115. Fidder, H., Knoester, J., and Wiersma, D. A. Optical properties of disordered molecular aggregates: A numerical study. *J. Chem. Phys.*, 1991, **95**, 7880–7890.
116. Wendling, M., Pullerits, T., Przyjalgowski, M. A., Vulto, S. I. E., Aartsma, T. J., van Grondelle, R., et al. Electron−vibrational coupling in the fenna−matthews−olson complex of prosthecochloris aestuarii determined by temperature-dependent absorption and fluorescence line-narrowing measurements. *J. Phys. Chem. B*, 2000, **104**, 5825–5831.
117. Hayes, J. M., Gillie, J. K., Tang, D., and Small, G. J. Theory for spectral hole burning of the primary electron donor state of photosynthetic reaction centers. *Biochim. Biophys. Acta Bioenergetics*, 1988, **932**, 287–305.
118. Pajusalu, M., Rätsep, M., and Freiberg, A. Temperature dependent electron–phonon coupling in chlorin-doped impurity glass and in photosynthetic fmo protein containing bacteriochlorophyll a. *J. Lumin.*, 2014, **152**, 79–83.
119. Miller, M., Cox, R. P., and Olson, J. M. Low-temperature spectroscopy of isolated fmo-protein and a membrane-free reaction center complex from the green sulfur bacterium chlorobium tepidum. *Photosynth. Res.*, 1994, **41**, 97.
120. Hayes, J. M., Lyle, P. A., and Small, G. J. A theory for the temperature dependence of hole-burned spectra. *J. Phys. Chem.*, 1994, **98**, 7337–7341.

121. Lyle, P. A., Kolaczkowski, S. V., and Small, G. J. Photochemical hole-burned spectra of protonated and deuterated reaction centers of rhodobacter sphaeroides. *J. Phys. Chem.*, 1993, **97**, 6924–6933.
122. Reddy, N. R. S., Kolaczkowski, S. V., and Small, G. J. Nonphotochemical hole burning of the reaction center of rhodopseudomonas viridis. *J. Phys. Chem.*, 1993, **97**, 6934–6940.
123. Pieper, J., Rätsep, M., Jankowiak, R., Irrgang, K. D., Voigt, J., Renger, G., et al. Qy-level structure and dynamics of solubilized light-harvesting complex ii of green plants: Pressure and hole burning studies. *J. Phys. Chem. A*, 1999, **103**, 2412–2421.
124. Angulo, G., Grampp, G., and Rosspeintner, A. Recalling the appropriate representation of electronic spectra. *Spectrochim. Acta A Mol. Biomol. Spectrosc.*, 2006, **65**, 727–731.
125. Freiberg, A., Timpmann, K., and Trinkunas, G. Spectral fine-tuning in excitonically coupled cyclic photosynthetic antennas. *Chem. Phys. Lett.*, 2010, **500**, 111–115.
126. Avarmaa, R. and Rebane, K. *Proc. Estonian SSR Acad. Sci.*, 1973, **22**, 108
127. Monshouwer, R., Abrahamsson, M., van Mourik, F., and van Grondelle, R. Superradiance and exciton delocalization in bacterial photosynthetic light-harvesting systems. *J. Phys. Chem. B*, 1997, **101**, 7241–7248.
128. Urboniene, V., Vrublevskaja, O., Trinkunas, G., Gall, A., Robert, B., and Valkunas, L. Solvation effect of bacteriochlorophyll excitons in light-harvesting complex lh2. *Biophysical J.*, 2007, **93**, 2188–2198.
129. Zerlauskiene, O., Trinkunas, G., Gall, A., Robert, B., Urboniene, V., and Valkunas, L. Static and dynamic protein impact on electronic properties of light-harvesting complex lh2. *J. Phys. Chem. B*, 2008, **112**, 15883–15892.
130. Wu, H.-M., Rätsep, M., Jankowiak, R., Cogdell, R. J., and Small, G. J. Comparison of the lh2 antenna complexes of *rhodopseudomonas acidophila* (strain 10050) and *rhodobacter sphaeroides* by high-pressure absorption, high-pressure hole burning, and temperature-dependent absorption spectroscopies. *J Phys. Chem. B*, 1997, **101**, 7641–7653.
131. Timpmann, K., Ellervee, A., Kuznetsov, A., Laisaar, A., Trinkunas, G., and Freiberg, A. Self-trapped excitons in lh2 bacteriochlorophyll-protein complexes under high pressure. *J. Lumin.*, 2003, **102–103**, 220–225.
132. Yano, R., Mitsunaga, M., Uesugi, N., and Shimizu, M. Temperature dependence of the homogeneous width of eu^{3+} spectral lines in silicate glass measured by accumulated photon echoes. *Phys. Rev. B*, 1994, **50**, 9031–9034.
133. Naumov, A. V., Vainer, Y. G., and Kador, L. Frequency dependence of the quadratic electron-phonon coupling constant in a polymer glass: Direct measurement by single-molecule spectroscopy. *Phys. Rev. B*, 2009, **79**, 132201.

134. Geva, E. and Skinner, J. L. Two-pulse photon echoes from zinc-meso-tetraphenylporphine/polymethylmethacrylate are not consistent with the tunneling two-level system model. *J. Chem. Phys.*, 1998, **108**, 8485–8488.
135. Geva, E. and Skinner, J. L. Optical line shapes of single molecules in glasses: Temperature and scan-time dependence. *J. Chem. Phys.*, 1998, **109**, 4920–4926.
136. Naumov, A. V., Vainer, Y. G., and Zilker, S. J. Nonexponential two-pulse photon echo decay in amorphous solids at low temperatures. *J. Lumin.*, 2000, **86**, 273–278.
137. Rätsep, M., Cai, Z.-L., Reimers, J. R., and Freiberg, A. Demonstration and interpretation of significant asymmetry in the low-resolution and high-resolution q_y fluorescence and absorption spectra of bacteriochlorophyll a. *J. Chem. Phys.*, 2011, **134**, 024506–024515.
138. Renge, I., Rätsep, M., and Freiberg, A. Intermolecular repulsive–dispersive potentials explain properties of impurity spectra in soft solids. *J. Lumin.*, 2011, **131**, 262–265.
139. Zazubovich, V., Tibe, I., and Small, G. J. Bacteriochlorophyll a franck-condon factors for the s0 → s1(qy) transition. *J. Phys. Chem. B*, 2001, **105**, 12410–12417.
140. Linnanto, J. M. and Korppi-Tommola, J. E. I. Modelling excitonic energy transfer in the photosynthetic unit of purple bacteria. *Chem. Phys.*, 2009, **357**, 171–180.
141. Beekman, L. M. P., Frese, R. N., Fowler, G. J. S., Picorel, R., Cogdell, R. J., van Stokkum, I. H. M., et al. Characterization of the light-harvesting antennas of photosynthetic purple bacteria by stark spectroscopy. 2. Lh2 complexes: Influence of the protein environment. *J. Phys. Chem. B*, 1997, **101**, 7293–7301.
142. Rätsep, M., Wu, H. M., Hayes, J. M., Blankenship, R. E., Cogdell, R. J., and Small, G. J. Stark hole-burning studies of three photosynthetic complexes. *J. Phys. Chem. B*, 1998, **102**, 4035–4044.
143. Timpmann, K., Ellervee, A., Pullerits, T., Ruus, R., Sundström, V., and Freiberg, A. Short-range exciton couplings in lh2 photosynthetic antenna proteins studied by high hydrostatic pressure absorption spectroscopy. *J. Phys. Chem. B*, 2001, **105**, 8436–8444.
144. Cory, M. G., Zerner, M. C., Hu, X., and Schulten, K. Electronic excitations in aggregates of bacteriochlorophylls. *J. Phys. Chem. B*, 1998, **102**, 7640–7650.
145. Levenberg, K. A method for the solution of certain non-linear problems in least squares. *Quart. Appl. Math.*, 1944, **2**, 164–168.
146. Kell, A., Acharya, K., Blankenship, R. E., and Jankowiak, R. On destabilization of the fenna–matthews–olson complex of chlorobaculum tepidum. *Photosynth. Res.*, 2014, **120**, 323–329.

147. Lu, X. and Pearlstein, R. M. Simulations of prosthecochloris bacteriochlorophyll a-protein optical spectra improved by parametric computer search. *Photochem. Photobiol.*, 1993, **57**, 86–91.
148. Beenken, W. J. D., Dahlbom, M., Kjellberg, P., and Pullerits, T. Potential surfaces and delocalization of excitons in dimers. *J. Chem. Phys.*, 2002, **117**, 5810–5820.

PUBLICATIONS

CURRICULUM VITAE

Name: Mihkel Pajusalu
Date of birth: 28.03.1986, Tartu, Estonia
Citizenship: Estonian
Contact: Ravila 14c-D111, 50411, Tartu, Estonia, (+372) 5381 5711, mihkel.pajusalu@ut.ee / mihkel.pajusalu@gmail.com

Education:

2005–2008	University of Tartu B. Sc. in physics *cum laude*
2008–2010	University of Tartu M. Sc. in physics *cum laude*

Professional career:

2006–2007	University of Tartu, Faculty of Philosophy, Department of Estonian and Fenno-Ugric studies, programmer
2007	University of Tartu, Faculty of Science and Technology, Institute of Physics, lab assistant
2011–	University of Tartu, Institute of Physics, engineer

Awards and stipends:

2009	Stipend for visiting the workgroup of Dr Gediminas Trinkunas (ESF DoRa program action 8: participation of young scientists in international knowledge exchange)
2009	University of Tartu, Institute of Physics student stipend
2009	First prize in the Estonian national students' research contest for bachelor's work (field of natural sciences and engineering, category of vocational higher education and bachelor students)
2010	University of Tartu, Institute of Physics student stipend
2010	University of Tartu Raefond's stipend
2010	First prize in the Estonian Academy of Science's student's research contest for master's thesis
2010	Third prize in the Estonian national students' research contest for master's thesis (field of natural sciences and engineering, category of MSc students)
2012	Kristjan Jaak program's stipend to attend the 11th International Conference on Hole Burning, Single Molecule and Related Spectroscopies: Science and Applications
2013	Ch. Villmann fellowship (space technology) from Tartu Observatory for work on the ESTCube-1 electrical power system

List of Publications:

Related to the Ph. D. thesis:

1. Rätsep, M.; Pajusalu, M.; Freiberg, A. (2009). Wavelength-dependent electron–phonon coupling in impurity glasses. Chemical Physics Letters, 479 (2009) 140.
2. Pajusalu, M.; Rätsep, M.; Trinkunas, G.; Freiberg, A. (2011). Davydov splitting of excitons in cyclic bacteriochlorophyll a nanoaggregates of bacterial light-harvesting complexes between 4.5 and 263 K. ChemPhysChem, 12(3), 634–644.
3. Freiberg, A.; Pajusalu, M.; Rätsep, M. (2013) Excitons in Intact Cells of Photosynthetic Bacteria. Journal of Physical Chemistry B, 117 (38), 11007–11014.
4. Pajusalu, M; Rätsep, M.; Freiberg, A. (2014) Temperature dependent electron–phonon coupling in chlorin-doped impurity glass and in photosynthetic FMO protein containing bacteriochlorophyll a. Journal of Luminescence, 152, 79–83.

Unrelated to the Ph. D. thesis:

5. Tkaczyk, E.R.; Mauring, T.; Pajusalu, M.; Anijalg, A.; Tkaczyk, A.; Teesalu, P.; Kikas, J.; Mauring, K. (2011). Cataract diagnosis by measurement of backscattered light. Optics Letters, 36(23), 4707–4709.
6. Pajusalu, M.; Rantsus, R.; Pelakauskas, M.; Leitu, A.; Ilbis, E.; Kalde, J.; Lillmaa, H.; Reinumägi, R.; Voormansik, K.; Zālīte, K.; Allik, V.; Noorma, M.; Lätt, S. (2012). Design of the electrical power system for the ESTCube-1 satellite. Latvian Journal of Physics and Technical Sciences, 49 (3), 16–24.
7. Pajusalu, Mihkel; Ilbis, Erik; Ilves, Taavi; Veske, Mihkel; Kalde, Jaanus;Lillmaa, Henri;Rantsus, Ramon; Pelakauskas, Martynas; Leitu, Ahto; Voormansik, Kaupo; Allik, Viljo; Lätt, Silver; Envall, Jouni; Noorma, Mart (2014). Design and pre-flight testing of the electrical power system for ESTCube-1 nanosatellite. Proceedings of the Estonian Academy of Sciences, 63 (2S), 232–241.
8. Envall, Jouni; Janhunen, Pekka; Toivainen, Petri; Pajusalu, Mihkel; Ilbis, Erik; Kalde, Jaanus; Averin, Matis; Kuuste, Henri; Laizans, Kaspars; Allik, Viljo; Rauhala, Timo; Seppänen, Henri; Kiprich, Sergiy; Ukkonen, Jukka; Haeggström, Edward; Kalvas, Taneli; Tarvainen, Olli; Kauppiainen, Janne; Nuottajärvi, Antti; Koivisto, Hannu (2014). E-sail test payload of the ESTCube-1 nanosatellite. Proceedings of the Estonian Academy of Sciences, 63 (2S), 210–221.
9. Lätt, Silver; Slavinskis, Andris; Ilbis, Erik; Kvell, Urmas; Voormansik, Kaupo; Kulu, Erik; Pajusalu, Mihkel; Kuuste, Henri; Sünter, Indrek; Eenmäe, Tõnis; Laizans, Kaspars; Zalite, Karlis; Vendt, Riho; Piepenbrock, Johannes; Ansko, Ilmar; Leitu, Ahto; Vahter, Andres; Agu, Ants; Eilonen, Elo; Soolo, Endel; Ehrpais, Hendrik; Lillmaa, Henri; Mahhonin, Ivar;

Mõttus, Jaak; Viru, Jaan; Kalde, Jaanus; Šubitidze, Jana; Mucenieks, Jānis; Šate, Jānis; Kütt, Johan; Poļevskis, Juris; Laks, Jürgen; Kivistik, Kadi; Kusmin, Kadri-Liis; Kruus, Kalle-Gustav; Tarbe, Karl; Tuude, Katrin; Kalniņa, Katrīna; Joost, Laur; Lõoke, Marko; Järve, Markus; Vellak, Mart; Neerot, Martin; Valgur, Martin; Pelakauskas, Martynas; Averin, Matis; Mikkor, Mats; Vaske, Mihkel; Scheler, Ott; Liias, Paul; Laes, Priit; Rantsus, Ramon; Soosaar, Reimo; Reinumägi, Risto; Valner, Robert; Kurvits, Siim; Mändmaa, Sven-Erik; Ilves, Taavi; Peet, Tanel; Ani, Tavo; Tilk, Teet; Tamm, Timothy Henry Charles; Scheffler, Tobias; Vahter, Toomas; Uiboupin, Tõnis; Evard, Veigo; Sisask, Andreas; Kimmel, Lauri; Krömer, Olaf; Rosta, Roland; Janhunen, Pekka; Envall, Jouni; Toivanen, Petri; Rauhala, Timo; Seppänen, Henri; Ukkonen, Jukka; Haeggström, Edward; Kurppa, Risto; Kalvas, Taneli; Tarvainen, Olli; Kauppinen, Janne; Nuottajärvi, Antti; Koivisto, Hannu; Kiprich, Sergiy; Obraztsov, Alexander; Allik, Viljo; Reinart, Anu; Noorma, Mart (2014). ESTCube-1 nanosatellite for electric solar wind sail in-orbit technology demonstration. Proceedings of the Estonian Academy of Sciences, 63(2S), 200–209.

International conference presentations related to the Ph. D. thesis:

2011 Poster at "Light Harvesting Processes 2011", "Temperature-Dependent Effects In LH2 Photosynthetic Antenna Complexes: Experiment And Theory"

2012 Oral presentation at Gordon Research Seminar: Electronic Processes in Organic Materials 2012 "Confirmation of presence of excitons in room-temperature bacterial cell membranes"

2012 Oral presentation at 11th International Conference on Hole Burning, Single Molecule and Related Spectroscopies "Exciton self-trapping in photosynthetic antennas revealed by single-molecule and exciton-state selective spectroscopies"

2012 Poster presentation at 11th International Conference on Hole Burning, Single Molecule and Related Spectroscopies "Temperature dependence of electron-phonon coupling in photosynthetic antennae"

2013 Oral prsentation at Light-Harvesting Processes 2013, "Studying Distribution of LH2 Complexes by Comparing Ensemble Studies and Single Molecule Spectra"

Supervised theses:

2011 Ramon Rantsus, M. Sc. thesis in computer engineering "Designing, Implementing and Testing the Solar Power Harvesting System for ESTCube-1," co-supervisor: Mart Noorma.

2011 Ahto Leitu, B. Sc. in computer engineering "Designing, Implementing and Testing the Power Distribution System for ESTCube-1," co-supervisor Mart Noorma.

2013 Henri Lillmaa, B. Sc. in computer engineering "Designing, building, programming and testing solar cell simulator for ESTCube-1".
2013 Taavi Ilves, M. Sc. thesis in computer engineering "ESTCube-1 electrical power system operation software," co-supervisor Mart Noorma.
2013 Erik Ilbis, B. Sc. in computer engineering "ESTCube-1 electrical power system – design, implementation and testing" (Received a prize in the Estonian Academy of Science's student's research contest and third prize in the Estonian national students' research contest).
2013 Juris Poļevskis (guest student from the Ventspils University College, Latvia), M. Sc. thesis "Nanosatelītu saules paneļu simulatora izstrāde" ("Developing a solar panel simulator for a nanosatellite", co-supervisor Andris Slavinskis)
2014 Rihor Raabe, B. Sc. thesis in physics "ESTCube-1 energy production simulator and analysis of telemetry data".
2014 Hannes Haljaste, B. Sc. in computer engineering "magnetic field simulator for ESTCube-1 testing," co-supervisor Viljo Allik.

Teaching:

2010/2011 autumn "LOFY.01.012 Practical Course in Physics II – Electricity and Magnetism (4 EAP)" practical co-supervisor
2011/2012 autumn "LOFY.01. Practical Course in Physics II – Electricity and Magnetism (4 EAP)" practical co-supervisor
2011/2012 autumn "LOFY.03.002 Computer Hardware II (3 EAP)" responsible lecturer
2012/2013 autumn "LOFY.01.012 Practical Course in Physics II – Electricity and Magnetism (4 EAP)" practical co-supervisor
2013/2014 autumn "LOFY.01.012 Practical Course in Physics II – Electricity and Magnetism (4 EAP)" and "LOFY.01.123 Practical Course in Physics II – Electricity and Magnetism (5 EAP)" practical co-supervisor

Public and social activities:

Team instructor for robotics competition Robotex 2007–2011
Jury member of the Estonian Physics Olympiad 2009–
Jury member of the Estonian Science Olympiad 2010–

- Estonian team mentor at EUSO (European Union Science Olympiad) 2012, IJSO (International Junior Science Olympiad) 2011, IJSO 2012, IJSO 2013

Member of the Estonian Seminatural Community Conservation Association 2010–

ELULOOKIRJELDUS

Nimi: Mihkel Pajusalu
Sünniaeg: 28.03.1986, Tartu, Eesti
Kodakondsus: Eesti
Kontakt: Ravila 14c-D111, 50411, Tartu, Eesti, (+372) 5381 5711, mihkel.pajusalu@ut.ee / mihkel.pajusalu@gmail.com

Haridus

2005–2008	Tartu Ülikool B. Sc. füüsikas *cum laude*
2008–2010	Tartu Ülikool M. Sc. füüsikas *cum laude*

Töökohad:

2006–2007	Tartu Ülikool, Filosoofiateaduskond, Eesti- ja Soome-Ugri keeleteaduse osakond, programmeerija
2007	Tartu Ülikooli Füüsika Instituut, laborant
2011–	Tartu Ülikooli Füüsika Instituut, insener

Preemiad ja stipendiumid:

2009	Stipendium Dr Gediminas Trinkunase töörühma külastamiseks (ESF DoRa programmi tegevus 8, Noorteadlaste osalemine rahvusvahelises teadmisteringluses)
2009	TÜ FI tudengistipendium
2009	I preemia üliõpilaste teadustööde riiklikul konkursil loodusteaduste ja tehnika valdkonnas rakenduskõrgharidusõppe ja bakalaureuseõppe üliõpilaste astmes
2010	TÜ FI tudengistipendium
2010	TÜ Raefondi stipendium
2010	I auhind Eesti Teaduste Akadeemia üliõpilaste teadustööde konkursil
2010	3. preemia üliõpilaste teadustööde riiklikul konkursil loodusteaduste ja tehnika valdkonnas magistriõppe üliõpilaste astmes
2012	Kristjan Jaagu välissõidu stipendium konverentsil 11th International Conference on Hole Burning, Single Molecule and Related Spectroscopies: Science and Applications osalemiseks
2013	Ch. Villmanni nimeline stipendium (kosmosetehnoloogia) Tartu Observatooriumilt ESTCube-1 elektrienergia alamsüsteemi arendamise eest

Publikatsioonid:

Doktoritööga seotud:

1. Rätsep, M.; Pajusalu, M.; Freiberg, A. (2009). Wavelength-dependent electron–phonon coupling in impurity glasses. Chemical Physics Letters, 479 (2009) 140
2. Pajusalu, M.; Rätsep, M.; Trinkunas, G.; Freiberg, A. (2011). Davydov splitting of excitons in cyclic bacteriochlorophyll a nanoaggregates of bacterial light-harvesting complexes between 4.5 and 263 K. ChemPhysChem, 12(3), 634–644.
3. Freiberg, A.; Pajusalu, M.; Rätsep, M. (2013) Excitons in Intact Cells of Photosynthetic Bacteria. Journal of Physical Chemistry B, 117 (38), 11007–11014.
4. Pajusalu, M; Rätsep, M.; Freiberg, A. (2014) Temperature dependent electron–phonon coupling in chlorin-doped impurity glass and in photosynthetic FMO protein containing bacteriochlorophyll a. Journal of Luminescence, 152, 79–83.

Doktoritööga mitteseotud:

5. Tkaczyk, E.R.; Mauring, T.; Pajusalu, M.; Anijalg, A.; Tkaczyk, A.; Teesalu, P.; Kikas, J.; Mauring, K. (2011). Cataract diagnosis by measurement of backscattered light. Optics Letters, 36(23), 4707–4709.
6. Pajusalu, M.; Rantsus, R.; Pelakauskas, M.; Leitu, A.; Ilbis, E.; Kalde, J.; Lillmaa, H.; Reinumägi, R.; Voormansik, K.; Zālīte, K.; Allik, V.; Noorma, M.; Lätt, S. (2012). Design of the electrical power system for the ESTCube-1 satellite. Latvian Journal of Physics and Technical Sciences, 49 (3), 16–24.
7. Pajusalu, Mihkel; Ilbis, Erik; Ilves, Taavi; Veske, Mihkel; Kalde, Jaanus;Lillmaa, Henri; Rantsus, Ramon; Pelakauskas, Martynas; Leitu, Ahto; Voormansik, Kaupo; Allik, Viljo; Lätt, Silver; Envall, Jouni; Noorma, Mart (2014). Design and pre-flight testing of the electrical power system for ESTCube-1 nanosatellite. Proceedings of the Estonian Academy of Sciences, 63 (2S), 232–241.
8. Envall, Jouni; Janhunen, Pekka; Toivainen, Petri; Pajusalu, Mihkel; Ilbis, Erik; Kalde, Jaanus; Averin, Matis; Kuuste, Henri; Laizans, Kaspars; Allik, Viljo; Rauhala, Timo; Seppänen, Henri; Kiprich, Sergiy; Ukkonen, Jukka; Haeggström, Edward; Kalvas, Taneli; Tarvainen, Olli; Kauppiainen, Janne; Nuottajärvi, Antti; Koivisto, Hannu (2014). E-sail test payload of the ESTCube-1 nanosatellite. Proceedings of the Estonian Academy of Sciences, 63 (2S), 210–221.
9. Lätt, Silver; Slavinskis, Andris; Ilbis, Erik; Kvell, Urmas; Voormansik, Kaupo; Kulu, Erik; Pajusalu, Mihkel; Kuuste, Henri; Sünter, Indrek; Eenmäe, Tõnis; Laizans, Kaspars; Zalite, Karlis; Vendt, Riho; Piepenbrock, Johannes; Ansko, Ilmar; Leitu, Ahto; Vahter, Andres; Agu, Ants; Eilonen, Elo; Soolo, Endel; Ehrpais, Hendrik; Lillmaa, Henri; Mahhonin, Ivar;

Mõttus, Jaak; Viru, Jaan; Kalde, Jaanus; Šubitidze, Jana; Mucenieks, Jānis; Šate, Jānis; Kütt, Johan; Poļevskis, Juris; Laks, Jürgen; Kivistik, Kadi; Kusmin, Kadri-Liis; Kruus, Kalle-Gustav; Tarbe, Karl; Tuude, Katrin; Kalniņa, Katrīna; Joost, Laur; Lõoke, Marko; Järve, Markus; Vellak, Mart; Neerot, Martin; Valgur, Martin; Pelakauskas, Martynas; Averin, Matis; Mikkor, Mats; Vaske, Mihkel; Scheler, Ott; Liias, Paul; Laes, Priit; Rantsus, Ramon; Soosaar, Reimo; Reinumägi, Risto; Valner, Robert; Kurvits, Siim; Mändmaa, Sven-Erik; Ilves, Taavi; Peet, Tanel; Ani, Tavo; Tilk, Teet; Tamm, Timothy Henry Charles; Scheffler, Tobias; Vahter, Toomas; Uiboupin, Tõnis; Evard, Veigo; Sisask, Andreas; Kimmel, Lauri; Krömer, Olaf; Rosta, Roland; Janhunen, Pekka; Envall, Jouni; Toivanen, Petri; Rauhala, Timo; Seppänen, Henri; Ukkonen, Jukka; Haeggström, Edward; Kurppa, Risto; Kalvas, Taneli; Tarvainen, Olli; Kauppinen, Janne; Nuottajärvi, Antti; Koivisto, Hannu; Kiprich, Sergiy; Obraztsov, Alexander; Allik, Viljo; Reinart, Anu; Noorma, Mart (2014). ESTCube-1 nanosatellite for electric solar wind sail in-orbit technology demonstration. Proceedings of the Estonian Academy of Sciences, 63(2S), 200–209.

Doktoritööga seotud ettekanded rahvusvahelistel konverentsidel:

2011 Posterettekanne konverentsil "Light Harvesting Processes 2011", "Temperature-Dependent Effects In LH2 Photosynthetic Antenna Complexes: Experiment And Theory"

2012 Suuline ettekanne konverentsil Gordon Research Seminar: Electronic Processes in Organic Materials 2012 "Confirmation of presence of excitons in room-temperature bacterial cell membranes"

2012 Suuline ettekanne konverentsil 11th International Conference on Hole Burning, Single Molecule and Related Spectroscopies "Exciton self-trapping in photosynthetic antennas revealed by single-molecule and exciton-state selective spectroscopies"

2012 Posterettekanne konverentsil 11th International Conference on Hole Burning, Single Molecule and Related Spectroscopies "Temperature dependence of electron-phonon coupling in photosynthetic antennae"

2013 Suuline ettekanne konverentsil Light-Harvesting Processes 2013, "Studying Distribution of LH2 Complexes by Comparing Ensemble Studies and Single Molecule Spectra"

Juhendatud lõputööd:

2011 Ramon Rantsus, arvutitehnika magistritöö "Designing, Implementing and Testing the Solar Power Harvesting System for ESTCube-1" (kaasjuhendaja: Mart Noorma)

2011 Ahto Leitu, arvutitehnika bakalaureusetöö "Designing, Implementing and Testing the Power Distribution System for ESTCube-1" (kaas-juhendaja Mart Noorma)

2013 Henri Lillmaa, arvutitehnika bakalaureusetöö “ESTCube-1 päikese-elemendi simulaatori arendus ja testimine”
2013 Taavi Ilves, arvutitehnika magistritöö “ESTCube-1 electrical power system operation software” (kaasjuhendaja Mart Noorma)
2013 Erik Ilbis, arvutitehnika bakalaureusetöö “ESTCube-1 electrical power system -design, implementation and testing” (Preemia Teaduste Akadeemia üliõpilastööde konkursil ja II preemia üliõpilaste teadustööde riiklikul konkursil)
2013 Juris Poļevskis (külalisüliõpilane Ventspilsi Kolledžist Lätist), magistritöö “Nanosatelītu saules paneļu simulatora izstrāde” (tõlkes “Nanosatelliidi päikesepaneeli simulaatori arendamine”, kaasjuhendaja Andris Slavinskis)
2014 Rihor Raabe, füüsika bakalauresusetöö “ESTCube-1 energiatootluse simulaator ja telemeetria andmete analüüs”
2014 Hannes Haljaste, arvutitehnika bakalaureusetöö “Magnetvälja simulaatori arendamine satelliidi ESTCube-1 testimiseks”, kaasjuhendaja Viljo Allik

Õpetamine:

2010/2011 sügis	“LOFY.01.012 Füüsika praktikum II – elekter ja magnetism (4 EAP)” praktikumi kaasjuhendaja
2011/2012 sügis	“LOFY.01.012 Füüsika praktikum II – elekter ja magnetism (4 EAP)” praktikumi kaasjuhendaja
2011/2012 sügis	“LOFY.03.002 Arvutiriistvara II (3 EAP)” aine vastutav õppejõud
2012/2013 sügis	“LOFY.01.012 Füüsika praktikum II – elekter ja magnetism (4 EAP)” praktikumi kaasjuhendaja
2013/2014 sügis	“LOFY.01.012 Füüsika praktikum II – elekter ja magnetism (4 EAP)” ja “LOFY.01.123 Füüsika praktikum II – elekter ja magnetism (5 EAP)” praktikumi kaasjuhendaja

Ühiskondlik tegevus:
Juhendaja robotivõistlusel Robotex 2007–2011
Eesti Füüsikaolümpiaadi žürii liige 2009–
Eesti Loodusteaduste olümpiaadi žürii liige 2010–

- Eesti võistkonna füüsika mentor EUSO (Euroopa Liidu loodusteaduste olümpiaad) 2012, IJSO (rahvusvaheline loodusteaduste olümpiaad) 2011, IJSO 2012, IJSO 2013

Pärandkoosluste kaitse ühingu liige 2010–

DISSERTATIONES PHYSICAE UNIVERSITATIS TARTUENSIS

1. **Andrus Ausmees.** XUV-induced electron emission and electron-phonon interaction in alkali halides. Tartu, 1991.
2. **Heiki Sõnajalg.** Shaping and recalling of light pulses by optical elements based on spectral hole burning. Tartu, 1991.
3. **Sergei Savihhin.** Ultrafast dynamics of F-centers and bound excitons from picosecond spectroscopy data. Tartu, 1991.
4. **Ergo Nõmmiste.** Leelishalogeniidide röntgenelektronemissioon kiiritamisel footonitega energiaga 70–140 eV. Tartu, 1991.
5. **Margus Rätsep.** Spectral gratings and their relaxation in some low-temperature impurity-doped glasses and crystals. Tartu, 1991.
6. **Tõnu Pullerits.** Primary energy transfer in photosynthesis. Model calculations. Tartu, 1991.
7. **Olev Saks.** Attoampri diapasoonis voolude mõõtmise füüsikalised alused. Tartu, 1991.
8. **Andres Virro.** AlGaAsSb/GaSb heterostructure injection lasers. Tartu, 1991.
9. **Hans Korge.** Investigation of negative point discharge in pure nitrogen at atmospheric pressure. Tartu, 1992.
10. **Jüri Maksimov.** Nonlinear generation of laser VUV radiation for high-resolution spectroscopy. Tartu, 1992.
11. **Mark Aizengendler.** Photostimulated transformation of aggregate defects and spectral hole burning in a neutron-irradiated sapphire. Tartu, 1992.
12. **Hele Siimon.** Atomic layer molecular beam epitaxy of A^2B^6 compounds described on the basis of kinetic equations model. Tartu, 1992.
13. **Tõnu Reinot.** The kinetics of polariton luminescence, energy transfer and relaxation in anthracene. Tartu, 1992.
14. **Toomas Rõõm.** Paramagnetic H^{2-} and F^+ centers in CaO crystals: spectra, relaxation and recombination luminescence. Tallinn, 1993.
15. **Erko Jalviste.** Laser spectroscopy of some jet-cooled organic molecules. Tartu, 1993.
16. **Alvo Aabloo.** Studies of crystalline celluloses using potential energy calculations. Tartu, 1994.
17. **Peeter Paris.** Initiation of corona pulses. Tartu, 1994.
18. **Павел Рубин.** Локальные дефектные состояния в CuO_2 плоскостях высокотемпературных сверхпроводников. Тарту, 1994.
19. **Olavi Ollikainen.** Applications of persistent spectral hole burning in ultrafast optical neural networks, time-resolved spectroscopy and holographic interferometry. Tartu, 1996.
20. **Ülo Mets.** Methodological aspects of fluorescence correlation spectroscopy. Tartu, 1996.
21. **Mikhail Danilkin.** Interaction of intrinsic and impurity defects in CaS:Eu luminophors. Tartu, 1997.

22. **Ирина Кудрявцева.** Создание и стабилизация дефектов в кристаллах KBr, KCl, RbCl при облучении ВУФ-радиацией. Тарту, 1997.
23. **Andres Osvet.** Photochromic properties of radiation-induced defects in diamond. Tartu, 1998.
24. **Jüri Örd.** Classical and quantum aspects of geodesic multiplication. Tartu, 1998.
25. **Priit Sarv.** High resolution solid-state NMR studies of zeolites. Tartu, 1998.
26. **Сергей Долгов.** Электронные возбуждения и дефектообразование в некоторых оксидах металлов. Тарту, 1998.
27. **Kaupo Kukli.** Atomic layer deposition of artificially structured dielectric materials. Tartu, 1999.
28. **Ivo Heinmaa.** Nuclear resonance studies of local structure in $RBa_2Cu_3O_{6+x}$ compounds. Tartu, 1999.
29. **Aleksander Shelkan.** Hole states in CuO_2 planes of high temperature superconducting materials. Tartu, 1999.
30. **Dmitri Nevedrov.** Nonlinear effects in quantum lattices. Tartu, 1999.
31. **Rein Ruus.** Collapse of 3d (4f) orbitals in 2p (3d) excited configurations and its effect on the x-ray and electron spectra. Tartu, 1999.
32. **Valter Zazubovich.** Local relaxation in incommensurate and glassy solids studied by Spectral Hole Burning. Tartu, 1999.
33. **Indrek Reimand.** Picosecond dynamics of optical excitations in GaAs and other excitonic systems. Tartu, 2000.
34. **Vladimir Babin.** Spectroscopy of exciton states in some halide macro- and nanocrystals. Tartu, 2001.
35. **Toomas Plank.** Positive corona at combined DC and AC voltage. Tartu, 2001.
36. **Kristjan Leiger.** Pressure-induced effects in inhomogeneous spectra of doped solids. Tartu, 2002.
37. **Helle Kaasik.** Nonperturbative theory of multiphonon vibrational relaxation and nonradiative transitions. Tartu, 2002.
38. **Tõnu Laas.** Propagation of waves in curved spacetimes. Tartu, 2002.
39. **Rünno Lõhmus.** Application of novel hybrid methods in SPM studies of nanostructural materials. Tartu, 2002.
40. **Kaido Reivelt.** Optical implementation of propagation-invariant pulsed free-space wave fields. Tartu, 2003.
41. **Heiki Kasemägi.** The effect of nanoparticle additives on lithium-ion mobility in a polymer electrolyte. Tartu, 2003.
42. **Villu Repän.** Low current mode of negative corona. Tartu, 2004.
43. **Алексей Котлов.** Оксианионные диэлектрические кристаллы: зонная структура и электронные возбуждения. Tartu, 2004.
44. **Jaak Talts.** Continuous non-invasive blood pressure measurement: comparative and methodological studies of the differential servo-oscillometric method. Tartu, 2004.
45. **Margus Saal.** Studies of pre-big bang and braneworld cosmology. Tartu, 2004.

46. **Eduard Gerškevitš.** Dose to bone marrow and leukaemia risk in external beam radiotherapy of prostate cancer. Tartu, 2005.
47. **Sergey Shchemelyov.** Sum-frequency generation and multiphoton ionization in xenon under excitation by conical laser beams. Tartu, 2006.
48. **Valter Kiisk.** Optical investigation of metal-oxide thin films. Tartu, 2006.
49. **Jaan Aarik.** Atomic layer deposition of titanium, zirconium and hafnium dioxides: growth mechanisms and properties of thin films. Tartu, 2007.
50. **Astrid Rekker.** Colored-noise-controlled anomalous transport and phase transitions in complex systems. Tartu, 2007.
51. **Andres Punning.** Electromechanical characterization of ionic polymer-metal composite sensing actuators. Tartu, 2007.
52. **Indrek Jõgi.** Conduction mechanisms in thin atomic layer deposited films containing TiO_2. Tartu, 2007.
53. **Aleksei Krasnikov.** Luminescence and defects creation processes in lead tungstate crystals. Tartu, 2007.
54. **Küllike Rägo.** Superconducting properties of MgB_2 in a scenario with intra- and interband pairing channels. Tartu, 2008.
55. **Els Heinsalu.** Normal and anomalously slow diffusion under external fields. Tartu, 2008.
56. **Kuno Kooser.** Soft x-ray induced radiative and nonradiative core-hole decay processes in thin films and solids. Tartu, 2008.
57. **Vadim Boltrushko.** Theory of vibronic transitions with strong nonlinear vibronic interaction in solids. Tartu, 2008.
58. **Andi Hektor.** Neutrino Physics beyond the Standard Model. Tartu, 2008.
59. **Raavo Josepson.** Photoinduced field-assisted electron emission into gases. Tartu, 2008.
60. **Martti Pärs.** Study of spontaneous and photoinduced processes in molecular solids using high-resolution optical spectroscopy. Tartu, 2008.
61. **Kristjan Kannike.** Implications of neutrino masses. Tartu, 2008.
62. **Vigen Issahhanjan.** Hole and interstitial centres in radiation-resistant MgO single crystals. Tartu, 2008.
63. **Veera Krasnenko.** Computational modeling of fluorescent proteins. Tartu, 2008.
64. **Mait Müntel.** Detection of doubly charged higgs boson in the CMS detector. Tartu, 2008.
65. **Kalle Kepler.** Optimisation of patient doses and image quality in diagnostic radiology. Tartu, 2009.
66. **Jüri Raud.** Study of negative glow and positive column regions of capillary HF discharge. Tartu, 2009.
67. **Sven Lange.** Spectroscopic and phase-stabilisation properties of pure and rare-earth ions activated ZrO_2 and HfO_2. Tartu, 2010.
68. **Aarne Kasikov.** Optical characterization of inhomogeneous thin films. Tartu, 2010.

69. **Heli Valtna-Lukner.** Superluminally propagating localized optical pulses. Tartu, 2010.
70. **Artjom Vargunin.** Stochastic and deterministic features of ordering in the systems with a phase transition. Tartu, 2010.
71. **Hannes Liivat.** Probing new physics in e+e− annihilations into heavy particles via spin orientation effects. Tartu, 2010.
72. **Tanel Mullari.** On the second order relativistic deviation equation and its applications. Tartu, 2010.
73. **Aleksandr Lissovski.** Pulsed high-pressure discharge in argon: spectroscopic diagnostics, modeling and development. Tartu, 2010.
74. **Aile Tamm.** Atomic layer deposition of high-permittivity insulators from cyclopentadienyl-based precursors. Tartu, 2010.
75. **Janek Uin.** Electrical separation for generating standard aerosols in a wide particle size range. Tartu, 2011.
76. **Svetlana Ganina.** Hajusandmetega ülesanded kui üks võimalus füüsikaõppe efektiivsuse tõstmiseks. Tartu, 2011
77. **Joel Kuusk.** Measurement of top-of-canopy spectral reflectance of forests for developing vegetation radiative transfer models. Tartu, 2011.
78. **Raul Rammula**. Atomic layer deposition of HfO_2 – nucleation, growth and structure development of thin films. Tartu, 2011.
79. **Сергей Наконечный.** Исследование электронно-дырочных и интерстициал-вакансионных процессов в монокристаллах MgO и LiF методами термоактивационной спектроскопии. Тарту, 2011.
80. **Niina Voropajeva.** Elementary excitations near the boundary of a strongly correlated crystal. Tartu, 2011.
81. **Martin Timusk.** Development and characterization of hybrid electro-optical materials. Tartu, 2012, 106 p.
82. **Merle Lust.** Assessment of dose components to Estonian population. Tartu, 2012, 84 p.
83. **Karl Kruusamäe.** Deformation-dependent electrode impedance of ionic electromechanically active polymers. Tartu, 2012, 128 p.
84. **Liis Rebane.** Measurement of the $W \to \tau\nu$ cross section and a search for a doubly charged Higgs boson decaying to τ-leptons with the CMS detector. Tartu, 2012, 156 p.
85. **Jevgeni Šablonin.** Processes of structural defect creation in pure and doped MgO and NaCl single crystals under condition of low or super high density of electronic excitations. Tartu, 2013, 145 p.
86. **Riho Vendt**. Combined method for establishment and dissemination of the international temperature scale. Tartu, 2013, 108 p.
87. **Peeter Piksarv.** Spatiotemporal characterization of diffractive and non-diffractive light pulses. Tartu, 2013, 156 p.
88. **Anna Šugai.** Creation of structural defects under superhigh-dense irradiation of wide-gap metal oxides. Tartu, 2013, 108 p.

89. **Ivar Kuusik.** Soft X-ray spectroscopy of insulators. Tartu, 2013, 113 p.
90. **Viktor Vabson**. Measurement uncertainty in Estonian Standard Laboratory for Mass. Tartu, 2013, 134 p.
91. **Kaupo Voormansik.** X-band synthetic aperture radar applications for environmental monitoring. Tartu, 2014, 117 p.
92. **Deivid Pugal.** hp-FEM model of IPMC deformation. Tartu, 2014, 143 p.
93. **Siim Pikker.** Modification in the emission and spectral shape of photostable fluorophores by nanometallic structures. Tartu, 2014, 98 p.